Electronic Supplementary Information

SO_2-resistant NO_x reduction over Cu-SAPO-34 catalysts via creating sulfur-phobic Cu sites

Jiebing He[†], Jiang Deng[†], Jin Zhang, Lupeng Han, Yongjie Shen, Xin Chen, Xiaonan Hu, Junan Wang[*], Dengsong Zhang[*]

State Key Laboratory of Advanced Special Steel, Institute of Materials, School of Materials Science and Engineering, International Joint Laboratory of Catalytic Chemistry, College of Sciences, Shanghai University, Shanghai 200444, China.

[†]These authors contributed equally to this paper.

*To whom correspondence should be addressed:

E-mail: dszhang@shu.edu.cn (DS Zhang); jawang@shu.edu.cn (JA Wang).

CONTENTS

Catalysts preparation

The conditions for HA of Cu-SAPO-34 catalyst at 700 and 900 ℃ are as follows: 2 g of Cu-SAPO-34 were placed into the muffle furnace. The target temperature was set at 700/900 °C for 1 h, and 10% water vapor was introduced when the temperature was raised to 700/900 °C, which was kept for 16 h. Then, the muffle furnace was naturally cooled down in the absence of water vapor. The samples were finally named as Cu-SAPO-34-A_2 and Cu-SAPO-34-A_3.

The sulfation treatment of the catalyst is as follows. The Cu-SAPO-34, Cu-SAPO-34-A_2, Cu-SAPO-34-A_3 and Cu-SAPO-34-A are pelletized through 40-60 mesh, then, 0.21 g of catalysts was placed in a quartz reaction tube. The temperature is raised to 300 °C for 20 min N_2 feed, and then 5 vol% O_2, 5 vol% H_2O, 40 ppm SO_2 and 50 ppm NH_3 are introduced when the temperature rises to 300 °C and the temperature is kept for 3h. The catalysts are finally labeled as Cu-SAPO-34-S, Cu-SAPO-34-A_2-S, Cu-SAPO-34-A_3-S and Cu-SAPO-34-A-S catalysts.

The sulfation treatment of the catalysts without NH_3 is similar to the above sulfation treatment, except that the sulfation treatment process only contains 5 vol% O_2, 5 vol% H_2O, and 40 ppm SO_2.

Catalysts characterization

The structure of catalysts was measured on an X-ray diffractometer (Rigaku D/MAS-RB) with Cu-Kα (40 kV, 40 mA) radiation, and the 2θ angles were recorded in the range of 5 ° to 80 ° with the scan speed of 8 °/min. UV-vis spectra were conducted on the Cary Series UV-Vis-NIR Spectrophotometer (Agilent Cary 5000). Thermogravimetric analysis used a Thermo scientific (TRACE 1300) model thermogravimetric analyzer. Hydrogen temperature-programmed reduction (H_2-TPR) was tested on a Micromeritics AutoChem 2920 II auto-adsorption apparatus with a thermal conductivity detector (TCD). Before the reduction process, 100 mg catalysts were pretreated under Ar atmosphere with a flow rate of 30 mL/min at 300 °C for 30 min, and then cooled to room temperature under Ar atmosphere. In H_2-TPR runs, the sample was exposed to 10% H_2/Ar and then the reactor temperature was raised from room temperature to 900 °C with a rate of 10 °C/min. The SO_2 breakthrough analysis of gas was carried out on a breakthrough analyzer (3P instrument mixSorb SHP). Before breakthrough analysis, 100 mg catalysts were pretreated under N_2 atmosphere with a flow rate of 30 mL/min for 30 min at 300 °C. When the temperature was fixed at 200/300 ℃ under nitrogen atmosphere, 0.4% SO_2/N_2 was introduced to the catalyst to proceed with the breakthrough analysis. The X-ray adsorption fine structure (XAFS) spectra (Cu K-edge) of various supported Cu catalysts and references (Cu foil and CuO_2) were collected at Bl14W1 beamline in Shanghai Synchrotron Radiation Facility (SSRF). The data was carried out in the transmission mode at ambient temperature.

In situ DRIFTS experiments

In situ DRIFTS was performed on the Nicolet 6700 spectrometer from Thermo Fisher Scientific of the United States with a mercury-cadmium-telluride (MCT/A) detector cooled by liquid nitrogen. The reaction cell (Harrick Scientific) was fitted with KBr windows and connected to a purging and adsorption gas control system. The powder sample in the reaction cell was treated under N_2 at 300 °C for 0.5 h to remove the surface impurities. Then the reaction cell was cooled to the target temperatures including 300, 250, 200, 150, 100, 50 and 30 °C. Background spectra were recorded at each target temperature. Afterwards, 1000 ppm NH_3/N_2 was used as the inlet gas for the reaction cell for 0.5 h, followed by purging with N_2 for another 10 min. The spectra were recorded by accumulating 64 scans with a resolution of 4 cm^{-1}. Nicolet 6700 spectrometer with reaction cell was also used to collect *in situ* DRIFTS spectra of $NO+O_2+(SO_2)$ on catalyst sample pretreated with NH_3 under 250 °C. The catalyst sample was preheated at 300 °C for 1 h in N_2, followed by collecting the background spectrum at each target temperature. The powder sample in the cell was firstly exposed to 1000 ppm NO+(1000 ppm SO_2)+5.0 % O_2/N_2 for 0.5 h and then used N_2 to purge for another 10 min. After that, the gas flow was switched to 1000 ppm NH_3/N_2 and the spectra were collected at 0, 5, 10, 15, 20, 25 and 30 min. Other transient reactions of $NO+O_2+(SO_2)$ on the catalyst sample pretreated with NH_3 were similar to *in situ* DRIFTS of NH_3 on catalyst sample pretreated with $NO+O_2+(SO_2)$.

The *in situ* pulsed infrared experiment is to pretreat the Cu-SAPO-34-S and Cu-SAPO-34-A-S under N_2 atmosphere at 300/350 °C for 30 min, and then lower the temperature to 250 °C for pulse experiment. The spectra were recorded by accumulating 32 scans with a resolution of 4 cm^{-1}, so the spectra were collected every 0.5 min. Firstly, pass in 1000 ppm NH_3 for 0~2.5 min, and then pass in 1000 ppm NO+5vol% O_2 at 2.5~5 min. We define 5 min of circulating NH_3/NO+O_2 as a reaction cycle, and continuous NH_3/NO+O_2 gas reaction for 10 cycles.

In situ Raman experiments

The Raman spectra were carried out on a LabRAM HR Evolution apparatus. The spectra were acquired in the range of 200~1300 cm^{-1} using a laser with a wavelength of 325 nm. The spectral resolution employed was 4 cm^{-1}. The *in situ* Raman test conditions were as follows. A small number of samples were placed in the *in situ* reaction cell, and the test laser was 325 nm ultraviolet light. At first, the spectrum was collected under N_2 atmosphere, and then slowly heated to 300 °C for pretreatment for 0.5 h. After the pretreatment, the temperature was lowered to 30 °C, 1000 ppm SO_2+5 vol% O_2 was introduced to react for 1 h, and then N_2 was introduced to purge for 10 min. Subsequently, the spectra at 30, 90, 150, 210, 270, 330 °C were collected during the continuous heating process.

In-situ UV-vis experiments

The spectrum collection range was 200~800 cm^{-1}, and the spectrum was collected every 2 min. The *in situ* UV-vis test conditions were as follows. A small number of samples were placed in the *in situ* reaction cell and placed on the *in situ* reaction table, and the temperature was raised to 300 °C for 30 min in a 5 vol% O_2/N_2 atmosphere. Then the temperature was lowered to 250 °C for *in situ* UV-vis experiments. Oxidation and reduction experiments was to firstly react for 30 min under 1000 ppm NO (1000 ppm SO_2)+5vol% O_2atmosphere, then cut off 1000 ppm NO (1000 ppm SO_2)+5 vol% O_2 and purged for 10 min under N_2 atmosphere, and finally introduced 1000 ppm NH_3 for reaction.

DFT Calculations

The calculations were carried out based on density functional theory (DFT) in the generalized gradient approximation (GGA) with the functional of Perdew, Burke and Ernzerh (PBE) [1] as implemented in the Vienna ab initio Simulation Package code (VASP 5.4.1) [2]. The $3d^{10}4s^1$, $3s^23p^4$, $3s^2p^1$, $2s^22p^2$, $2s^22p^3$, and $2s^22p^4$ of Cu, S, Al, Si, N, and O atoms were treated as valence electrons, respectively, and the remaining core electrons were represented by the Troullier-Martins norm conserving pseudopotentials [3]. SAPO-34 was modeled in its rhombohedral unit cell. All Cu-SAPO-34 periodic structures including different copper species (ZCuOH and Z_2Cu) are built in a 2 × 2 × 2 supercell. The Brillouin zone integration was performed using Monkhorst-Pack scheme with 1 × 1 × 1 k-points. The force and energy convergences were 0.02 eV/Å and 10^{-4} eV for geometry optimizations, respectively. Taking into change the ZCuOH into Z_2Cu by hydrothermal aging method, the Cu-SAPO-34 was modeled with the ZCuOH configuration, while the Cu-SAPO-34-A was modeled as Z_2Cu. Periodic boundary conditions were used for all systems. All calculations were spin polarized. The energy cutoff of 400 eV was chosen to guarantee convergence of the total energies and forces. All the calculations were performed at Γ point of the Brillouin zone. The adsorption energy for NH_3, NO and SO_2 molecules on Z_2Cu and ZCuOH was defined as $E_{ads}=E_{mol}@(Z_2Cu)-E(Z_2Cu)-E(mol)$, and the adsorption energy for these molecules on ZCuOH was defined as $E_{ads}= E_{mol}@(ZCuOH)-E(ZCuOH)-E(mol)$, where mol denotes NH_3, NO and SO_2 molecules.

Catalytic activity measurements

The evaluations of SCR activity were measured by using 0.21 g catalysts (40–60 mesh) in a fixed-bed reactor. The composition of mixed gas was: 500 ppm NO, 500 ppm NH_3, 5 vol % O_2 and 2.5 vol% H_2O in the N_2 balance. The gas concentrations of NO, NO_2, NH_3, H_2O, and N_2O were simultaneously monitored by an FTIR spectrometer (Thermo Fisher, ANTARIS IGS Analyzer). The total gas flow rate was 510 mL/min, which was corresponding to 100 000 h^{-1} gas hourly space velocity (GHSV). The NO conversion percentage was calculated using the formulas (1, 2):

$$\text{NO conversion}\ (\%) = \frac{[\text{NO}]_{\text{in}} - [\text{NO}]_{\text{out}}}{[\text{NO}]_{\text{in}}} \times 100\% \quad (1)$$

$$\text{N2 selectivity}\ (\%) = 1 - \frac{2[\text{N2O}]_{out}}{[\text{NO}]_{\text{in}} + [\text{NH3}]_{\text{in}} - [\text{NO}]_{\text{out}} - [\text{NH3}]_{\text{out}}} \times 100\% \quad (2)$$

where $[NO]_{in}$, $[NH_3]_{in}$, $[NO]_{out}$, $[NH_3]_{out}$ and $[N_2O]_{out}$ corresponded to the concentration of NO, NH_3 and N_2O in the inlet and outlet in a steady-state, respectively.

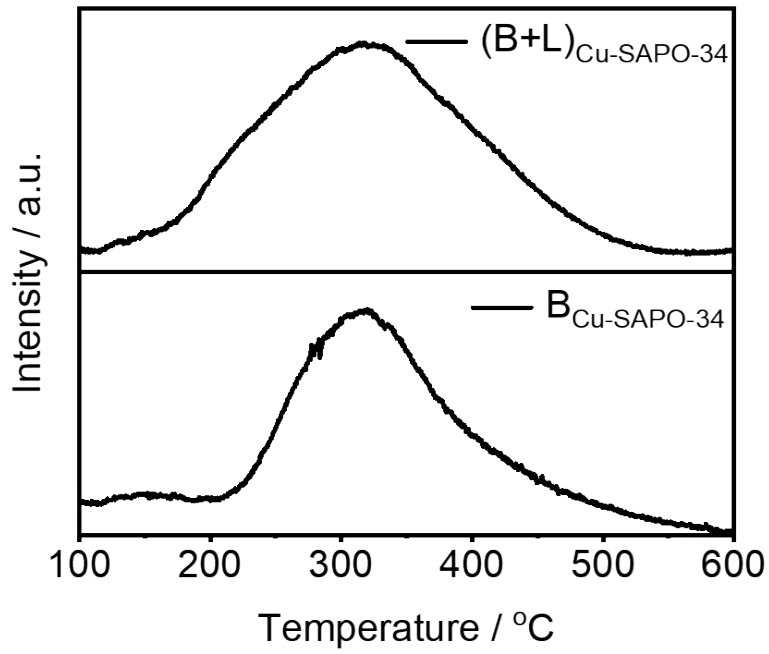

Figure S1. The contents of Z_2Cu and ZCuOH sites in the Cu-SAPO-34 catalyst via ammonia titration method. B stands for Bronsted acid sites and L stands for Lewis acid sites.

The results of ammonia titration show that the proportion of $-NH_2$ species adsorbed on the Z_2Cu sites for Cu-SAPO-34 is 13%, and the NH_4^+ species adsorbed on the ZCuOH sites is 87%. Studies have shown that Z_2Cu sites adsorb 4 molecules of NH_3 to form $Z_2Cu(NH_3)_4$, and ZCuOH sites adsorb 3 molecules of NH_3 to form $ZCu(NH_3)_3(OH)$. Therefore, it can be calculated that the contents of ZCuOH and Z_2Cu sites in the Cu-SAPO-34 is 90.0% and 10.0%, respectively.

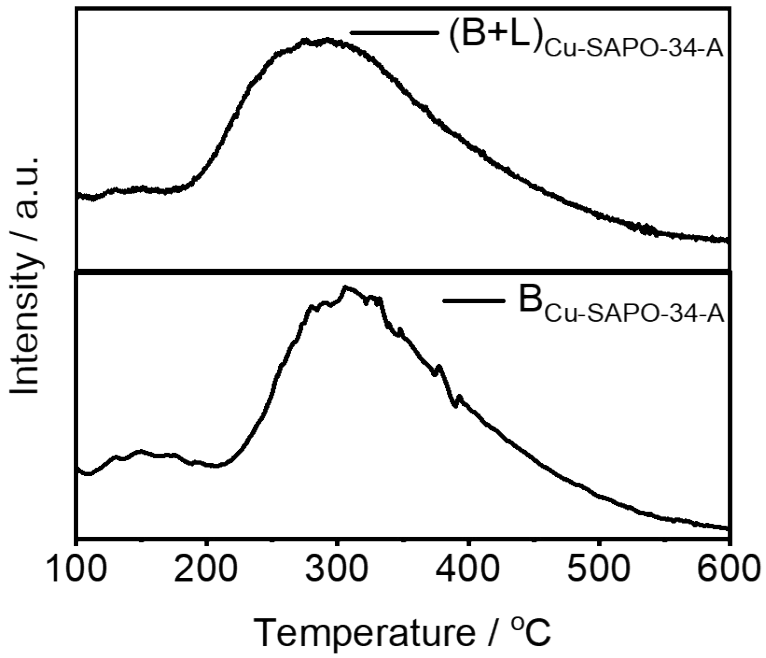

Figure S2. The contents of Z_2Cu and ZCuOH sites in the Cu-SAPO-34-A catalyst via ammonia titration method. B represents Bronsted acid sites and L represents Lewis acid sites.

The results of ammonia titration show that the proportion of NH_4^+ and -NH_2 species adsorbed on the ZCuOH and Z_2Cu sites for Cu-SAPO-34-A accounted for 71% and 29%, respectively. Studies have shown that Z_2Cu sites adsorb 4 molecules of NH_3 to form $Z_2Cu(NH_3)_4$, and ZCuOH sites adsorb 3 molecules of NH_3 to form $ZCu(NH_3)_3(OH)$. Therefore, the content of ZCuOH and Z_2Cu sites in the Cu-SAPO-34-A is 76.5% and 23.5%, respectively.

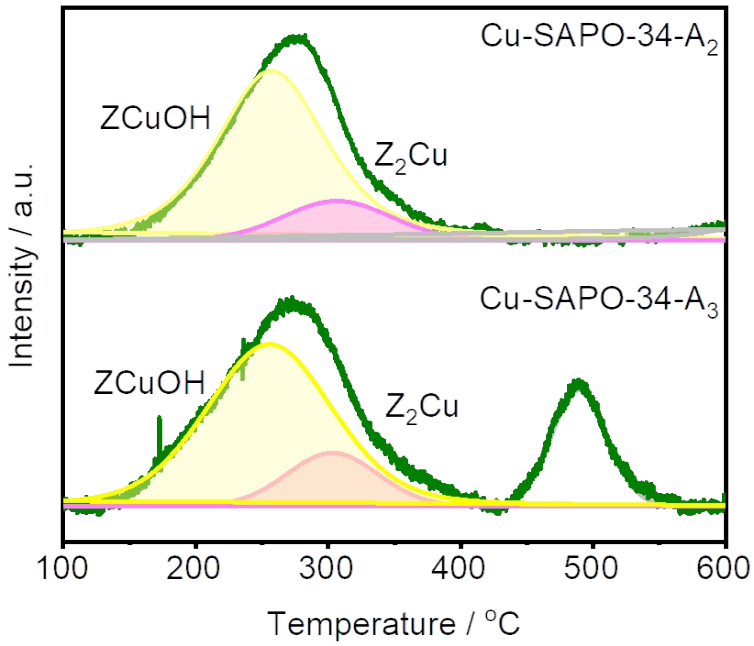

Figure S3. H_2-TPR profiles of Cu-SAPO-34-A_2 and Cu-SAPO-34-A_3 catalysts.

It can be seen from Figure S3 that both Cu-SAPO-34-A_2 and Cu-SAPO-34-A_3 have two reduction peaks at 200-400 ℃. The reduction peak at low temperature is attributed to the reduction at ZCuOH sites, and the reduction at high temperature is attributed to the reduction at Z_2Cu sites. By integrating the reduction peak area of catalyst Cu-SAPO-34-A_2 and Cu-SAPO-34-A_3, it can be seen that the content of ZCuOH sites and Z_2Cu sites in Cu-SAPO-34-A_2 is 84.0% and 16.0% respectively, and the content of ZCuOH sites and Z_2Cu sites in Cu-SAPO-34-A_2 is 81.8% and 18.2% respectively. Cu-SAPO-34-A_3 has a small reduction peak at 450-550 ℃, the attribution of this peak is still controversial in the existing research. Some researchers [4-6] believe that in the reduction of Cu-CHA catalyst, the reduction peak between 350-550 ℃ is attributed to the reduction of Z_2Cu site in the six-member ring. Some research [7-11]

concluded that the H_2-TPR reduction peak of Cu-CHA catalyst near 400-500 ℃ is the reduction from Cu^+ to Cu^0. Some researchers [12] also attributed the reduction peak at 400-600 ℃ to the reduction of $Cu_2Al_2O_4$ species. To sum up, the reduction peak of Cu-CHA catalyst at about 400-500 ℃ may be attributed to the reduction of Cu species in the six-member ring, the reduction of Cu^+ to Cu^0 and the reduction of $Cu_2Al_2O_4$ species. If a new $Cu_2Al_2O_4$ species reduction peak appears in the Cu-CHA, it indicates that the structure of the catalyst collapses, which shows the decline of NH_3-SCR activity at high temperature. In this manuscript, Cu-SAPO-34-A, Cu-SAPO-34-A_2, Cu-SAPO-34-A_3 and Cu-SAPO-34 maintained nearly 100% NO conversion at 270-480 ℃. Therefore, the reduction peak here is classified as the further reduction of Cu species in the six-member ring or the reduction of Cu^+ species to Cu^0 species.

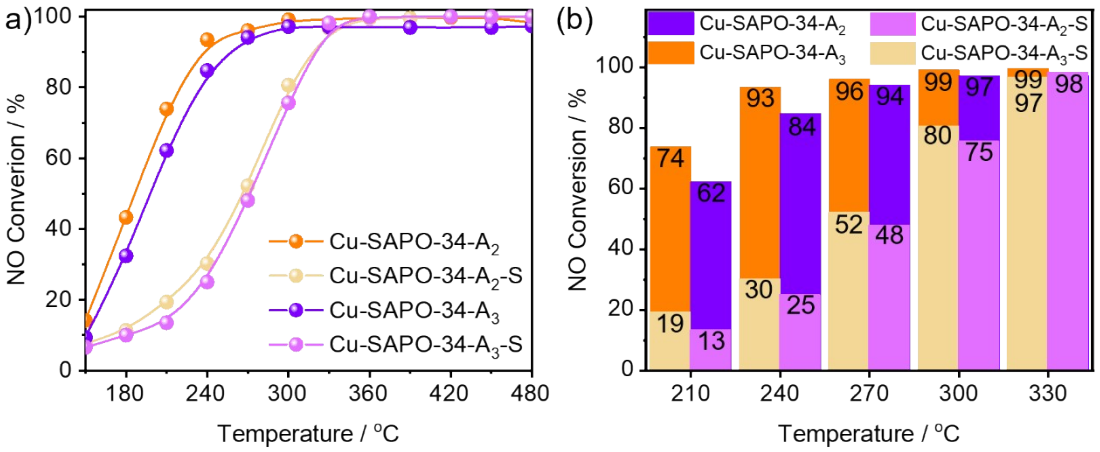

Figure S4. (a) Plots of NO conversion versus temperature for Cu-SAPO-34-A_2, Cu-SAPO-34-A_3, Cu-SAPO-34-A_2-S and Cu-SAPO-34-A_3-S catalysts, and (b) the NO conversion of Cu-SAPO-34-A_2, Cu-SAPO-34-A_3, Cu-SAPO-34-A_2-S and Cu-SAPO-34-A_3-S catalysts at different temperature. Reaction conditions: 500 ppm of NO, 500 ppm of NH_3, 5 vol % O_2, 2.5 vol % H_2O, N_2 as the balance gas, and GHSV of 100 000 h^{-1}.

Figure S4 shows the NH_3-SCR activity and SO_2-resistance of Cu-SAPO-34 treated at different hydrothermal aging temperatures. Cu-SAPO-34-A_2 showed more than 90% NO conversion at 240-480 ℃, and Cu-SAPO-34-A_3 showed lower NO conversion at 150-480 ℃ than Cu-SAPO-34-A_2, and the NO conversion was higher than 90% after reaching 270 ℃ (Figure S4a). Figure S4b shows the NO conversion of Cu-SAPO-34-A_2, Cu-SAPO-34-A_3, Cu-SAPO-34-A_2-S and Cu-SAPO-34-A_3-S at 210, 240, 270, 300 and 330 ℃. It can be seen that the NO conversion of Cu-SAPO-34-A_2 is higher than that of Cu-SAPO-34-A_3 at each temperature point, and the activity of Cu-SAPO-34-A_2-S is higher than that of Cu-SAPO-34-A_3-S.

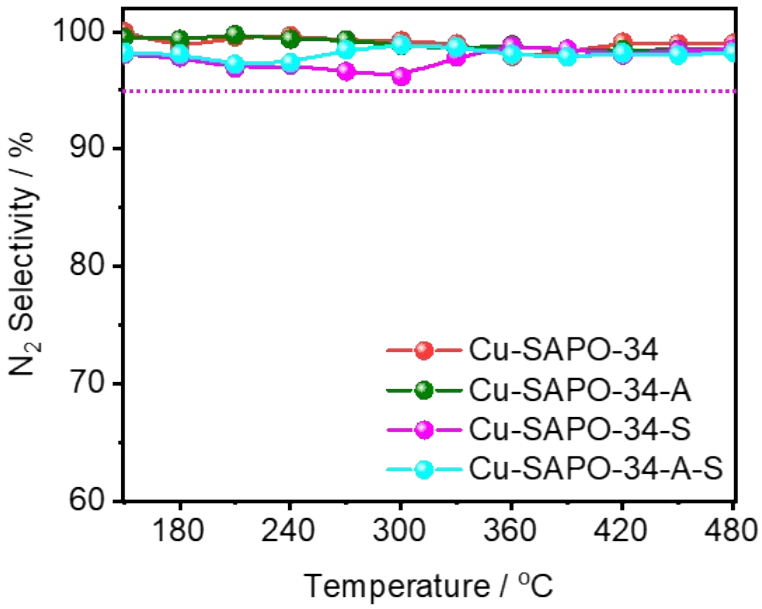

Figure S5. Plots of N_2 selectivity versus temperature for Cu-SAPO-34, Cu-SAPO-34-A, Cu-SAPO-34-S and Cu-SAPO-34-A-S catalysts. Reaction conditions: 500 ppm of NO, 500 ppm of NH_3, 5 vol % O_2, 2.5 vol % H_2O, N_2 as the balance gas, and GHSV of 100 000 h^{-1}.

Figure S5 shows the N_2 selectivity of NH_3-SCR reaction of Cu-SAPO-34, Cu-SAPO-34-A, Cu-SAPO-34-S and Cu-SAPO-34-A-S catalysts in the temperature window of 150-480 ℃. Only a small amount of N_2O is produced in the temperature window of 150-480 ℃ for Cu-SAPO-34 and Cu-SAPO-34-A catalysts, so their N_2 selectivity is always higher than 98%. The N_2 selectivity of the Cu-SAPO-34-S catalyst in the temperature window of 150-330 and 330-480 ℃ is not less than 96 and 98%, respectively. The N_2 selectivity of the Cu-SAPO-34-A-S catalyst in the temperature window of 150-270 and 270-480 ℃ is not less than 96 and 98%, respectively.

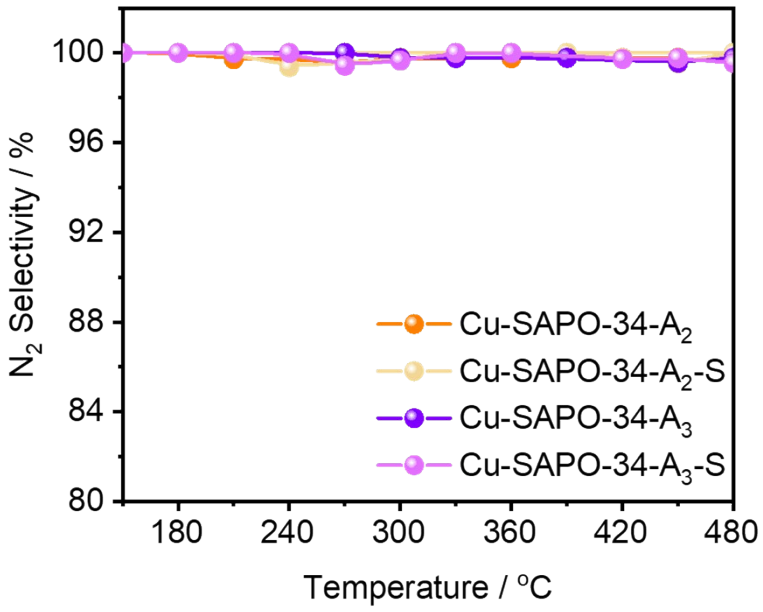

Figure S6. Plots of N_2 selectivity versus temperature for Cu-SAPO-34-A_2, Cu-SAPO-34-A_3, Cu-SAPO-34-A_2-S and Cu-SAPO-34-A_3-S catalysts. Reaction conditions: 500 ppm of NO, 500 ppm of NH_3, 5 vol % O_2, 2.5 vol % H_2O, N_2 as the balance gas, and GHSV of 100 000 h^{-1}.

Figure S6 shows that Cu-SAPO-34-A_2, Cu-SAPO-34-A_3, Cu-SAPO-34-A_2-S and Cu-SAPO-34-A_3-S have excellent N_2 selectivity in the temperature window of 150-480 °C.

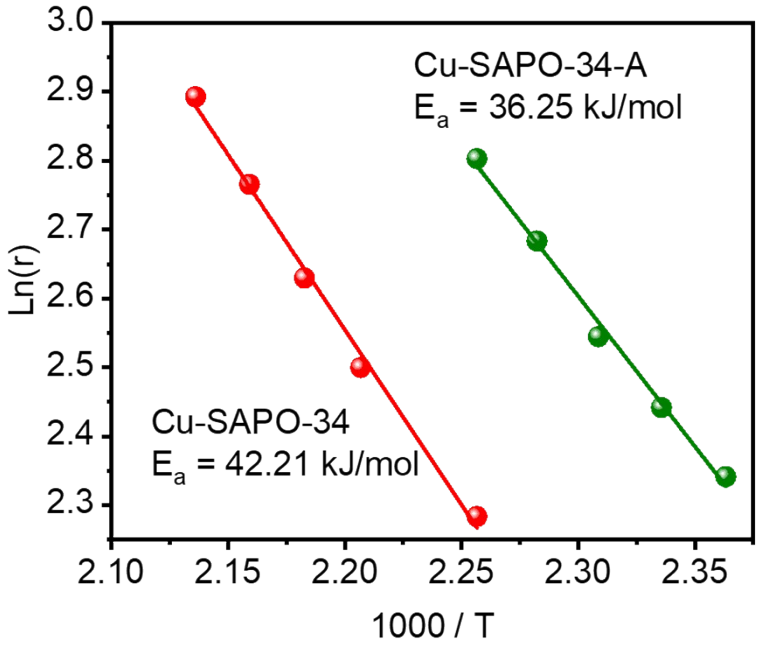

Figure S7. Arrhenius plots for SCR performance over the Cu-SAPO-34 and Cu-SAPO-34-A catalysts. Reaction conditions: 500 ppm of NO, 500 ppm of NH_3, 5 vol% O_2, N_2 as the balance gas, and GHSV of 400 000 h^{-1}

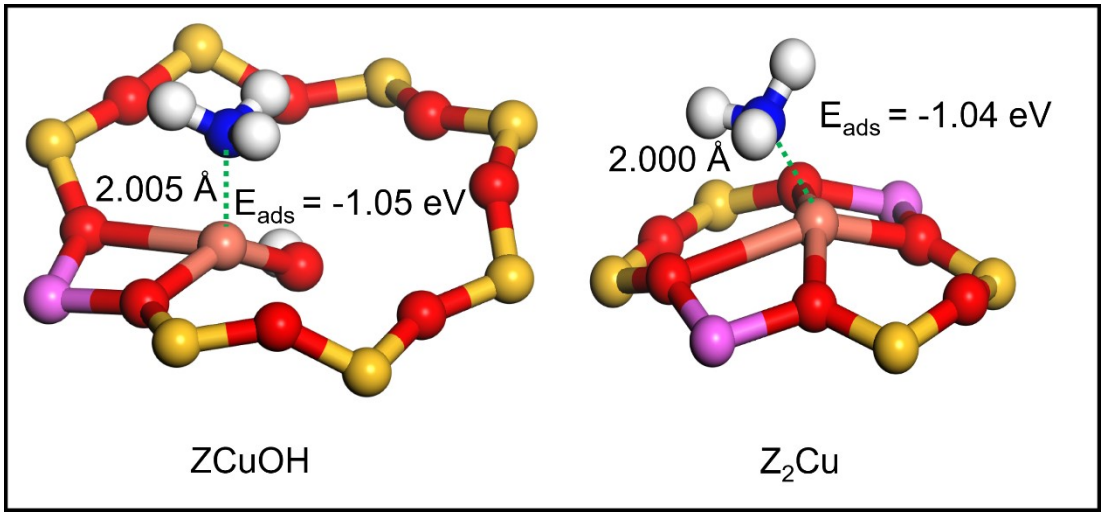

Figure S8. The most stable configuration of NH_3 on ZCuOH and Z_2Cu sites.

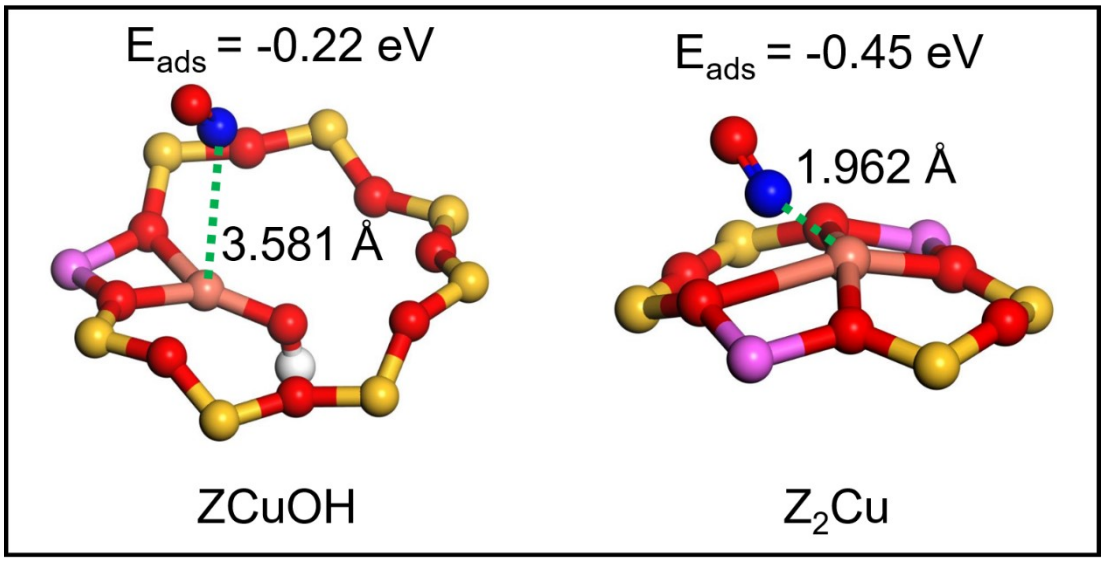

Figure S9. The most stable configuration of NO on ZCuOH and Z_2Cu sites.

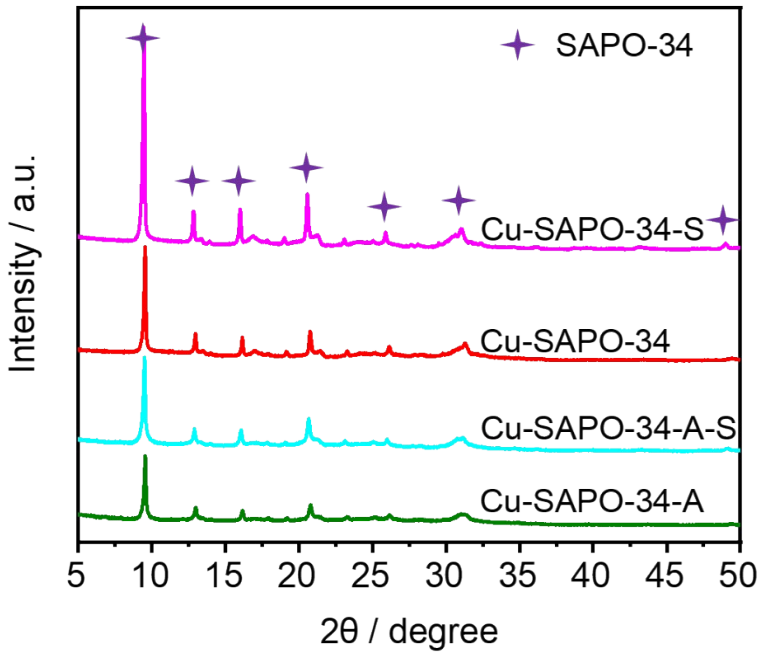

Figure S10. XRD patterns of Cu-SAPO-34, Cu-SAPO-34-S, Cu-SAPO-34-A and Cu-SAPO-34-A-S catalysts.

It can be seen from the XRD patterns that the Cu-SAPO-34, Cu-SAPO-34-S, Cu-SAPO-34-A and Cu-SAPO-34-A-S all maintain the zeolite crystal structure of SAPO-34, indicating that SO_2-poisoning does not damage the framework structure of the catalyst. At the same time, there is no obvious diffraction peak of sulfate species, indicating that there are no crystalline sulfate species.

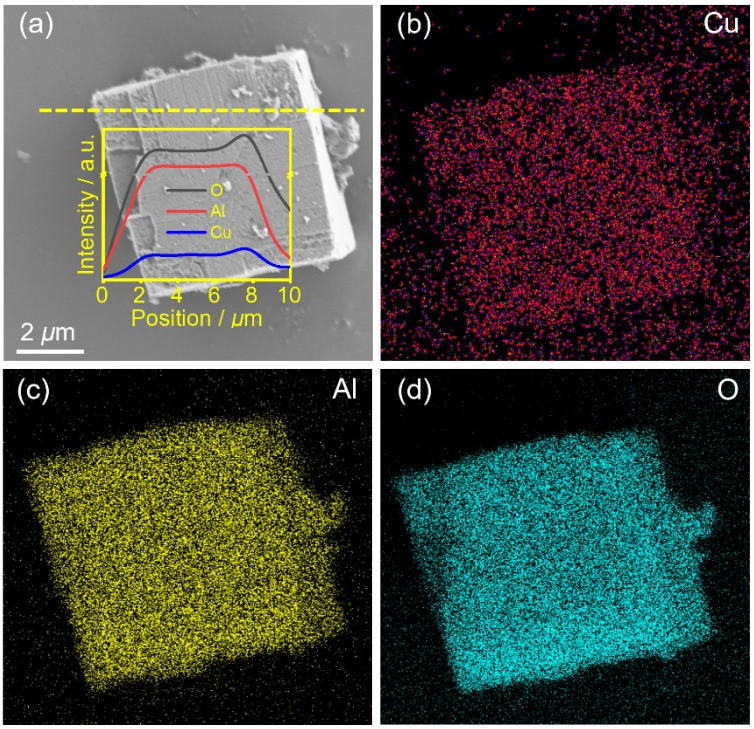

Figure S11. (a) SEM image of the Cu-SAPO-34-A catalyst (inset image represented the line scanning results of Cu, Al and O elements) and EDX mapping of the (b) Cu, (c) Al and (d) O elements over the Cu-SAPO-34-A catalyst.

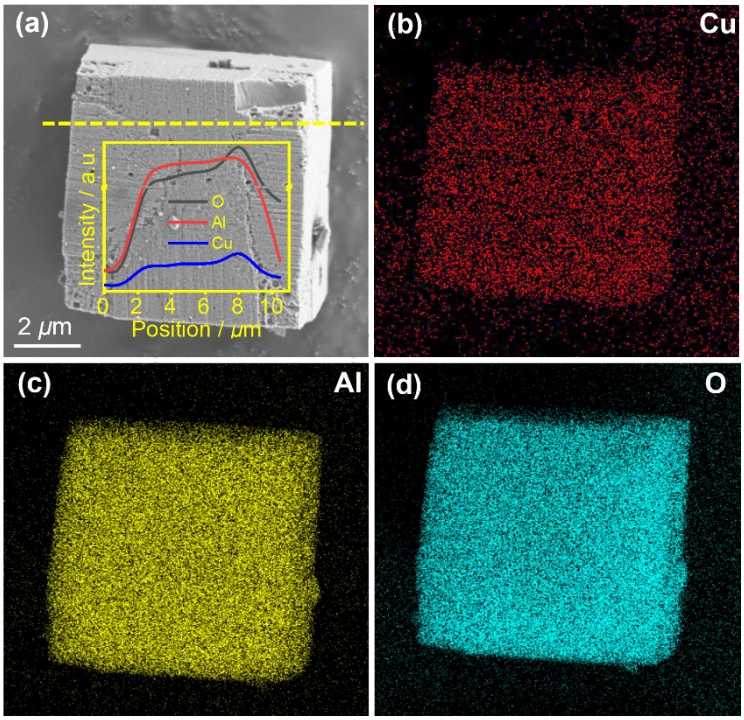

Figure S12. (a) SEM image of the Cu-SAPO-34 catalyst (inset image represented the line scanning results of Cu, Al and O elements) and EDX mapping of the (b) Cu, (c) Al and (d) O elements over the Cu-SAPO-34 catalyst.

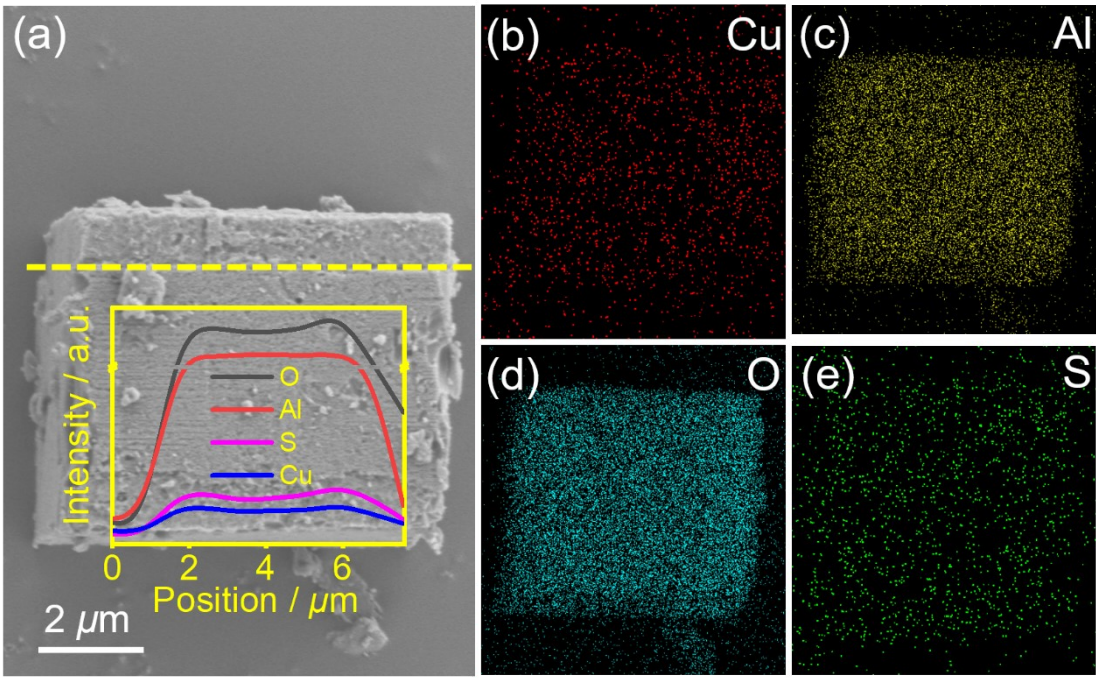

Figure S13. (a) SEM image of the Cu-SAPO-34-A-S catalyst (inset image represented the line scanning results of Cu, Al, O and S elements) and EDX mapping of the (b) Cu, (c) Al, (d) O and (e) S elements over the Cu-SAPO-34-A-S catalyst.

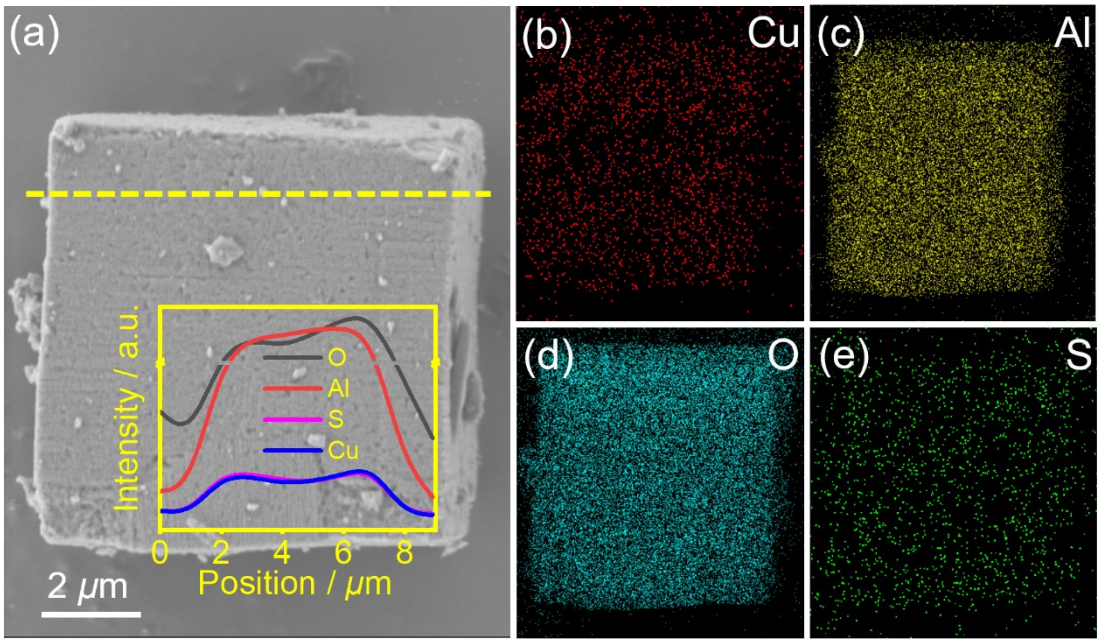

Figure S14. (a) SEM image of the Cu-SAPO-34-S catalyst (inset image represented the line scanning results of Cu, Al, O and S elements) and EDX mapping of the (b) Cu, (c) Al, (d) O and (e) S elements over the Cu-SAPO-34-S catalyst.

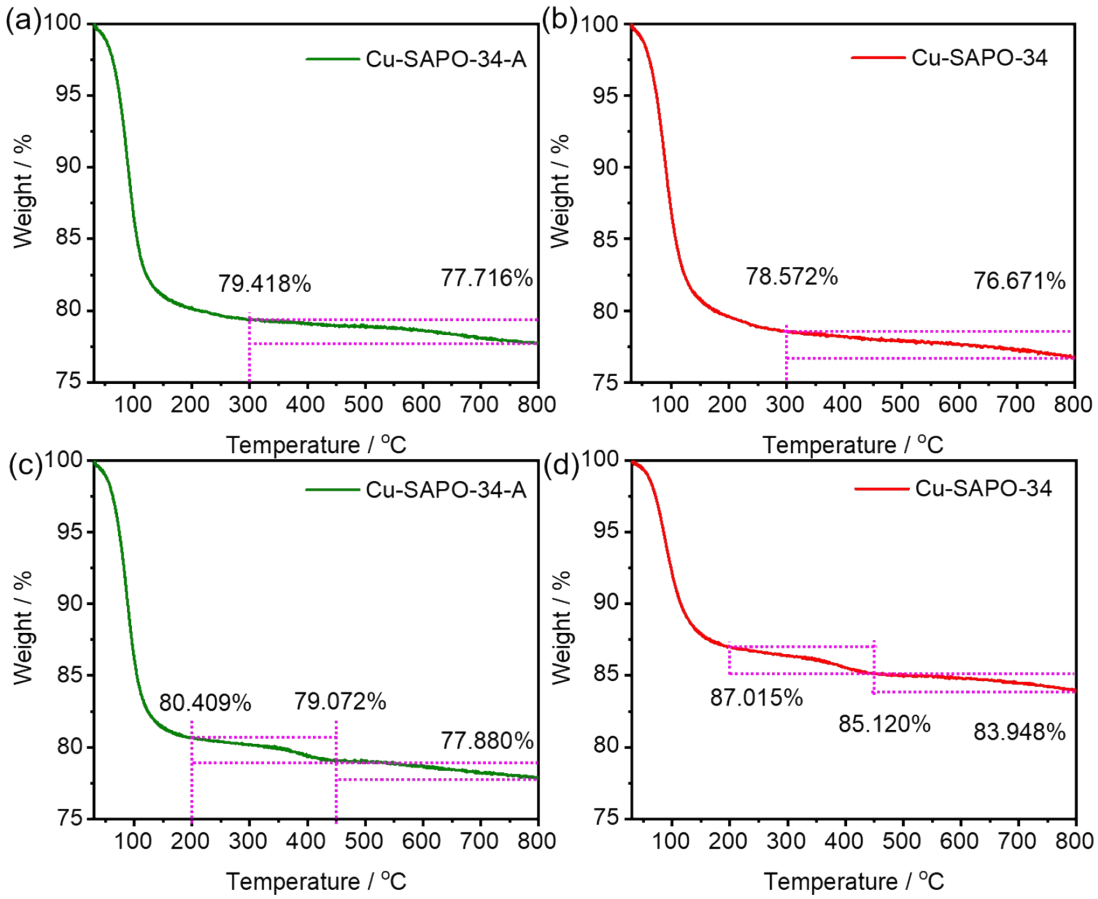

Figure S15. TG plots of Cu-SAPO-34-A (a) and Cu-SAPO-34 (b) catalysts poisoned in SO_2+H_2O+O_2 feed; TG plots of Cu-SAPO-34-A (c) and Cu-SAPO-34 (d) catalysts poisoned in SO_2+NH_3+H_2O+O_2 feed.

Firstly, the Cu-SAPO-34-A and Cu-SAPO-34 is SO_2-poisoned in a feed containing only SO_2+H_2O+O_2. Since there is no NH_3, only metal sulfate species are produced in this process. Preliminary calculations show that the amount of metal sulfate species produced on the Cu-SAPO-34-A and Cu-SAPO-34 is 17.0 mg/g and 19.0 mg/g, respectively (Figure S15a, S15b, Table S5). Afterwards, to further investigate the amount of produced ABS, the Cu-SAPO-34-A and Cu-SAPO-34 is SO_2 poisoned in an

$NH_3+SO_2+O_2+H_2O$ feed. Since ABS decomposes between 250~400 °C, the decomposition temperature of metal sulfate is higher than 500 °C. Therefore, from the loss of TG at different temperatures, it can be concluded that the production of ABS and metal sulfate species on the Cu-SAPO-34-A are 13.4 mg/g and 11.9 mg/g; while the production of ABS and metal sulfate species on the Cu-SAPO-34 are 19.0 mg/g and 11.9 mg/g (Figure S15c, S15d, Table S5). Cu-SAPO-34-A with more sulfur-phobic Z_2Cu sites generates less sulfate species than Cu-SAPO-34 under two different sulfation conditions of $SO_2+O_2+H_2O$ and $NH_3+SO_2+O_2+H_2O$. The formation of less sulfate species makes Cu-SAPO-34-A have more excellent resistance to SO_2 poisoning.

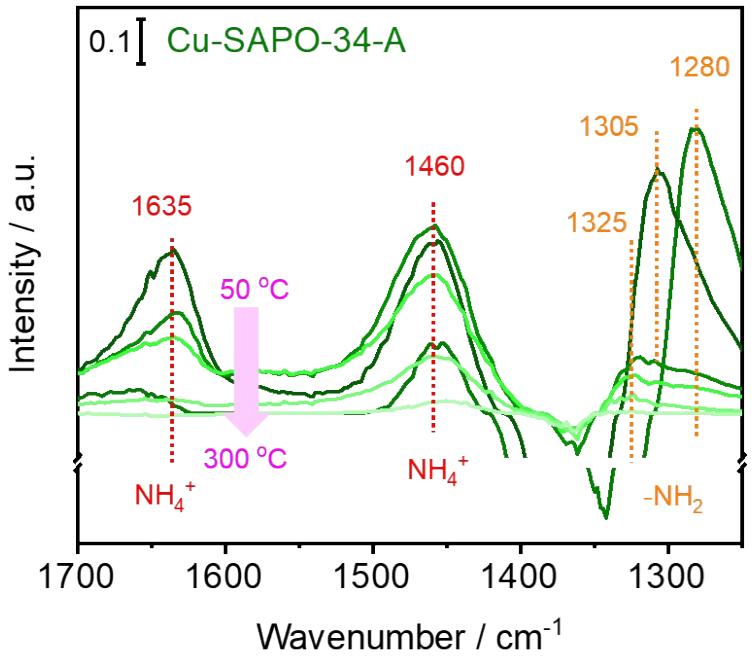

Figure S16. *In situ* DRIFTs of NH_3 desorption over Cu-SAPO-34-A catalyst as a function of temperature.

Firstly, the desorption behavior of NH_4^+ species and -NH_2 species under different temperature was compared by *in situ* absorption and desorption of NH_3. The ammonia species adsorbed on the Cu-SAPO-34-A mainly exist as -NH_2 (1280, 1305, 1325 cm^{-1}) and NH_4^+ (1460, 1635 cm^{-1}) [13-17]. The -NH_2 species adsorbed at 1280 cm^{-1} are classified as $[Cu^{2+}(NH_3)_4]^{2+}$, indicating that NH_3 could be adsorbed on the Z_2Cu sites. It can be seen from Figure S16 that as the temperatures increases, the peak at 1280 cm^{-1} shifts to a high wavenumber of 1305 cm^{-1}, or even to 1325 cm^{-1}. The adsorbed ammonia species at 1460 cm^{-1} represents the formation of NH_4^+ derived from NH_3 solvation. The formation of this solvated NH_4^+ species is coordinated with the Cu site of the Cu-CHA catalyst to enhance the mobility of the Cu site, so that the Cu-CHA catalyst maintains

excellent activity at low temperatures. The absorption peak of the NH_4^+ species at 1630 cm^{-1} represents N-H bend of Cu-NH_3, which can be inferred to be the ammonia species adsorbed on the ZCuOH sites (ZCuOH$(NH_3)_3$). It is interesting that the absorption peak of NH_4^+ species here also shifts to high wavenumbers as the temperature rises.

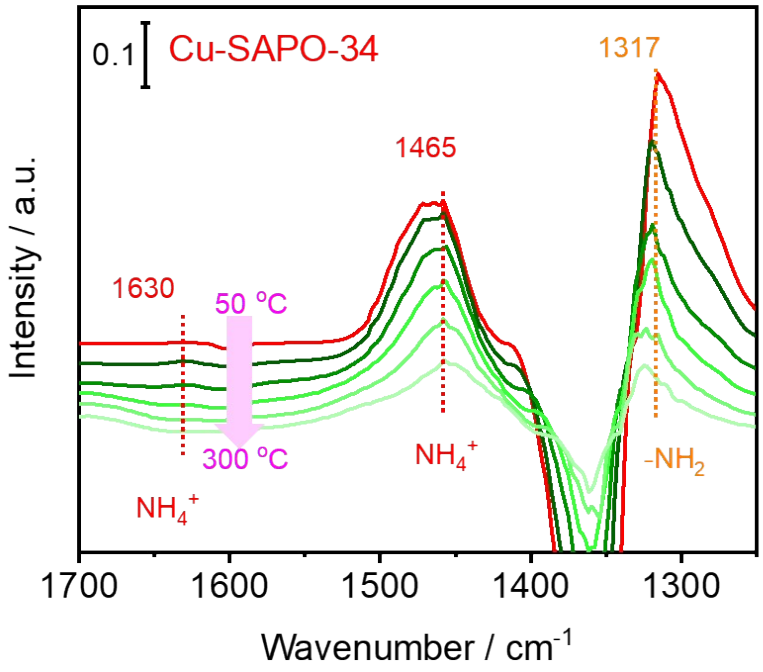

Figure S17. *In situ* DRIFTs of NH_3 desorption over Cu-SAPO-34 catalyst as a function of temperature.

Firstly, the desorption behavior of NH_4^+ species and -NH_2 species under different temperatures was compared by *in situ* absorption and desorption of NH_3. The ammonia species adsorbed on the Cu-SAPO-34 are mainly -NH_2 (1317 cm^{-1}) and NH_4^+ (1465, 1630 cm^{-1}). The -NH_2 species adsorbed at 1280 cm^{-1} is classified as $[Cu^{2+}(NH_3)_4]^{2+}$, indicating that it is ammonia adsorbed on the Z_2Cu sites. Comparing the NH_3 adsorption and desorption experiments of Cu-SAPO-34-A and Cu-SAPO-34, it is known that as the temperature increases, the -NH_2 species are easily desorbed. When the -NH_2 species desorbs more than half of it, the NH_4^+ species begins to desorb.

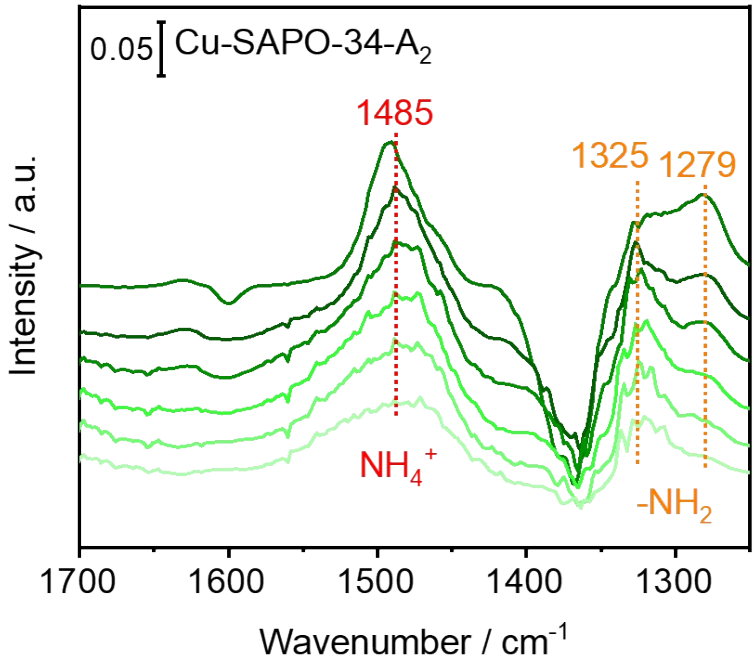

Figure S18. In situ DRIFTs of NH_3 desorption over Cu-SAPO-34-A_2 catalyst as a function of temperature.

The ammonia species adsorbed on Cu-SAPO-34-A_2 mainly exist in the form of NH_4^+ (1485 cm^{-1}) and -NH_2 (1325 and 1279 cm^{-1}) (Figure S18). As the desorption temperature rises to 300 ℃, the ammonia species are basically consumed, indicating that the ammonia species adsorbed on Cu-SAPO-34-A_2 has high reactivity.

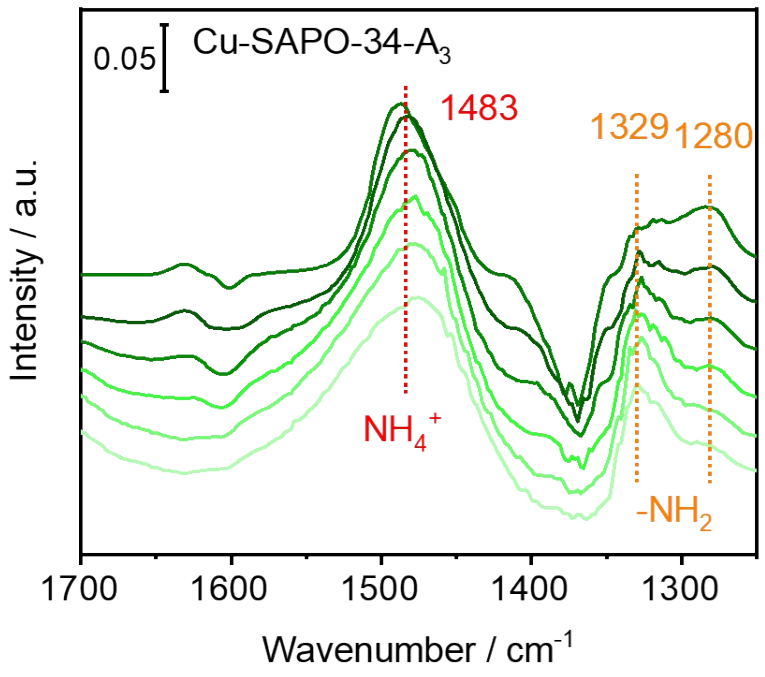

Figure S19. In situ DRIFTs of NH_3 desorption over Cu-SAPO-34-A_3 catalyst as a function of temperature.

Figure S19 shows that the ammonia species on Cu-SAPO-34-A_3 also exist in the form of NH_4^+ (1483 cm^{-1}) and -NH_2 (1329 and 1280 cm^{-1}), but with the increase of desorption temperature, -NH_2 species have a certain amount of desorption, and NH_4^+ species have only a small amount of desorption. It is shown that the reactivity of ammonia species adsorbed on Cu-SAPO-34-A_3 is poor due to ultra-high hydrothermal aging temperature (900 ℃).

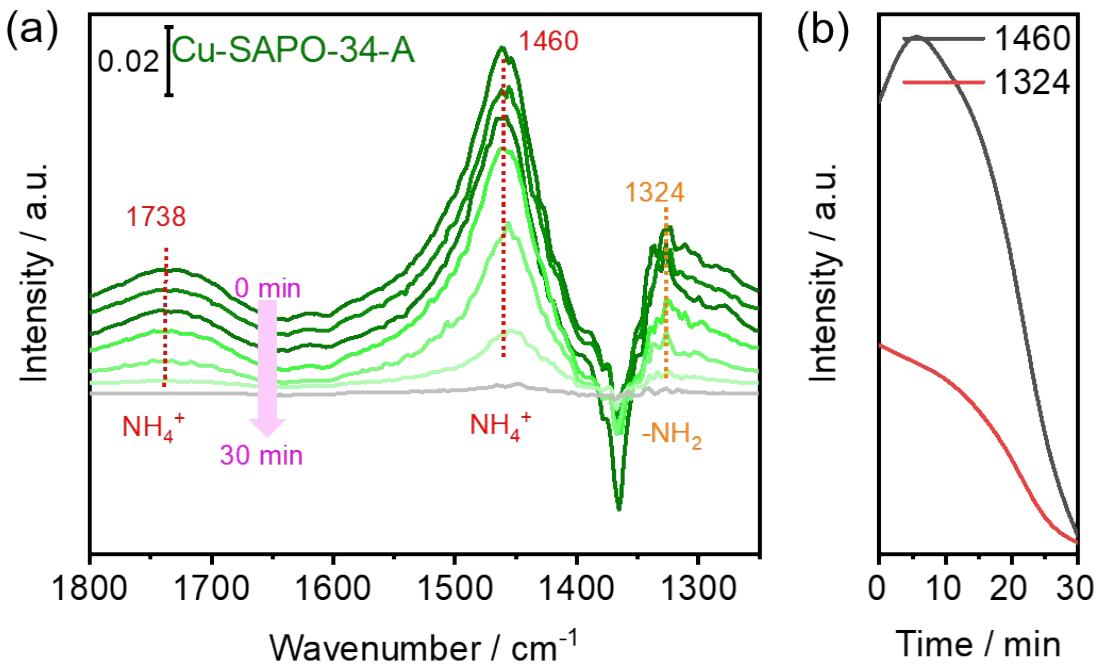

Figure S20. *In situ* DRIFTs of the transient reactions at 250 °C over Cu-SAPO-34-A catalyst between $NO+O_2$ (a) and preadsorbed NH_3 as a function of time. (b) Consumption of the bands at 1324 cm^{-1} and 1460 cm^{-1} over Cu-SAPO-34-A catalyst in Figure (a).

Firstly, the Cu-SAPO-34-A is adsorbed at 250 °C for 30 min of NH_3, and then $NO+O_2$ is introduced to react. After the Cu-SAPO-34-A adsorbs NH_3, it can be learned when $NO+O_2$ is introduced, that the-NH_2 species (1324 cm^{-1}) and the NH_4^+ species (1460 cm^{-1}) are consumed rapidly as the reaction time increases, until the reaction is complete. By the way, the short-term rise of the NH_4^+ species may be due to the re-adsorption of a small amount of desorbed ammonia species (Figure S20a, 20b).

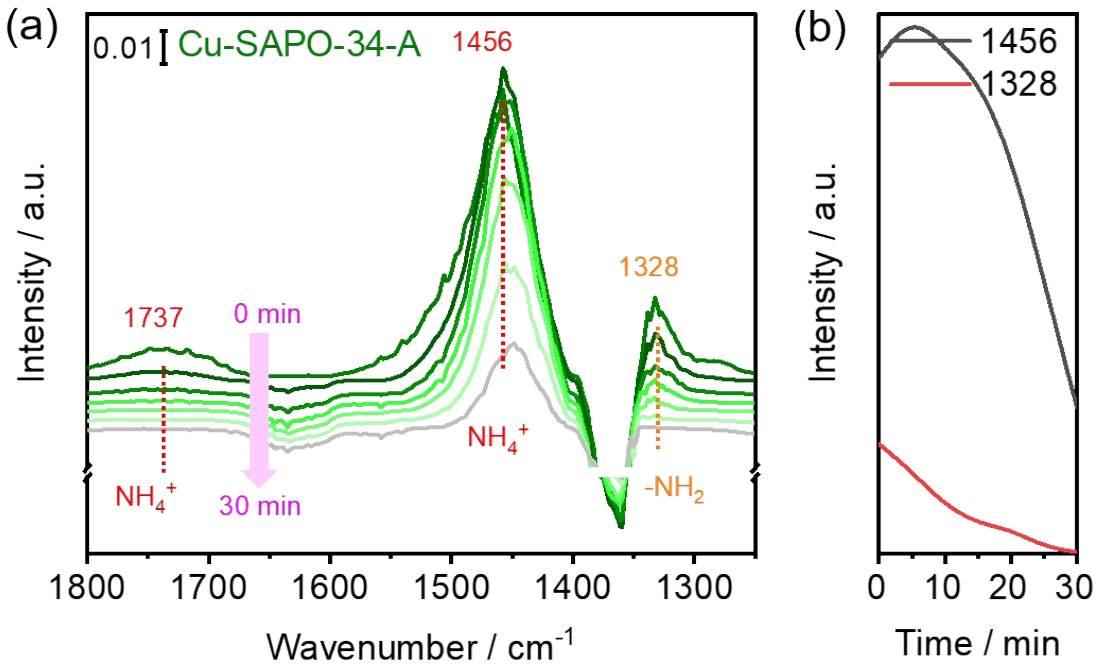

Figure S21. *In situ* DRIFTs of the transient reactions at 250 °C over Cu-SAPO-34-A catalyst between $NO+SO_2+O_2$ (a) and preadsorbed NH_3 as a function of time. (b) Consumption of the bands at 1328 cm^{-1} and 1456 cm^{-1} over Cu-SAPO-34-A catalysts in Figure (a).

Firstly, the Cu-SAPO-34-A is adsorbed at 250 °C for 30 min of NH_3, and then $NO+SO_2+O_2$ is introduced to react. When the Cu-SAPO-34-A is reacted with SO_2+NO+O_2 after adsorbing NH_3, the $-NH_2$ species (1328 cm^{-1}) still has a high reaction rate and the reaction is completed quickly; while the NH_4^+ species (1456 cm^{-1}) can also participate in the reaction, but the reaction rate becomes slower and unable to react completely (Figure S21a, 21b).

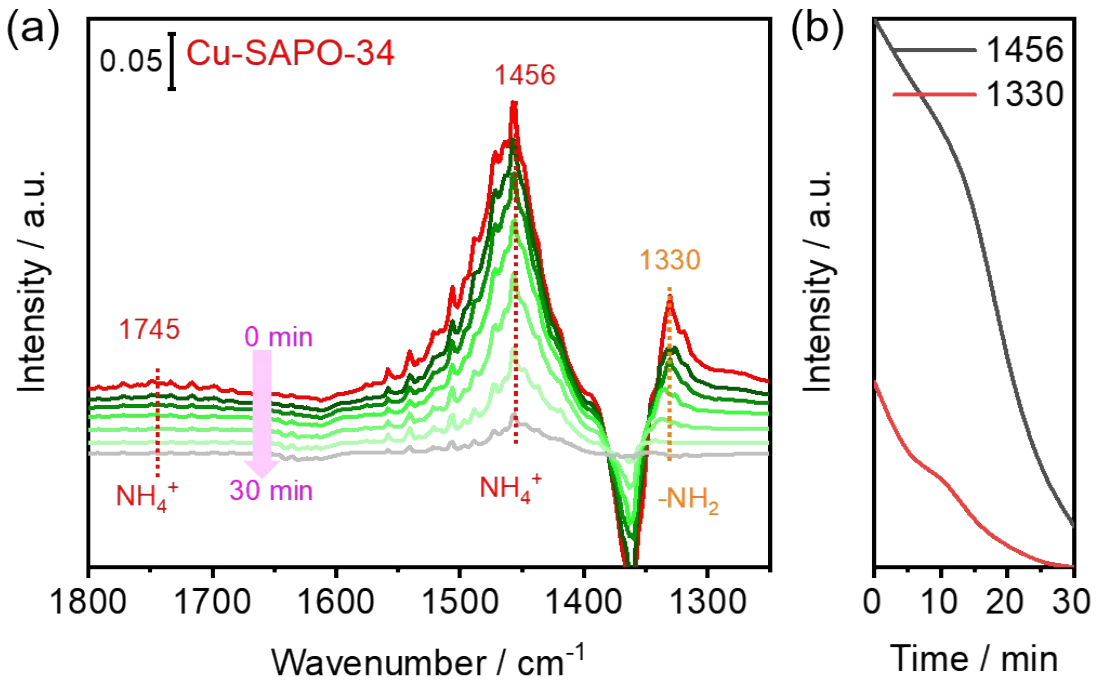

Figure S22. *In situ* DRIFTs of the transient reactions at 250 °C over Cu-SAPO-34 catalyst between $NO+O_2$ (a) and preadsorbed NH_3 as a function of time. (b) Consumption of the bands at 1330 cm^{-1} and 1456 cm^{-1} over Cu-SAPO-34 catalyst in Figure (a).

After the Cu-SAPO-34 adsorbs NH_3 and then enters the $NO+O_2$ reaction, it can also be detected that the $-NH_2$ species (1330 cm^{-1}) and the NH_4^+ species (1456 cm^{-1}) react quickly to complete consumption as the reaction time increases (Figure S22a, 22b).

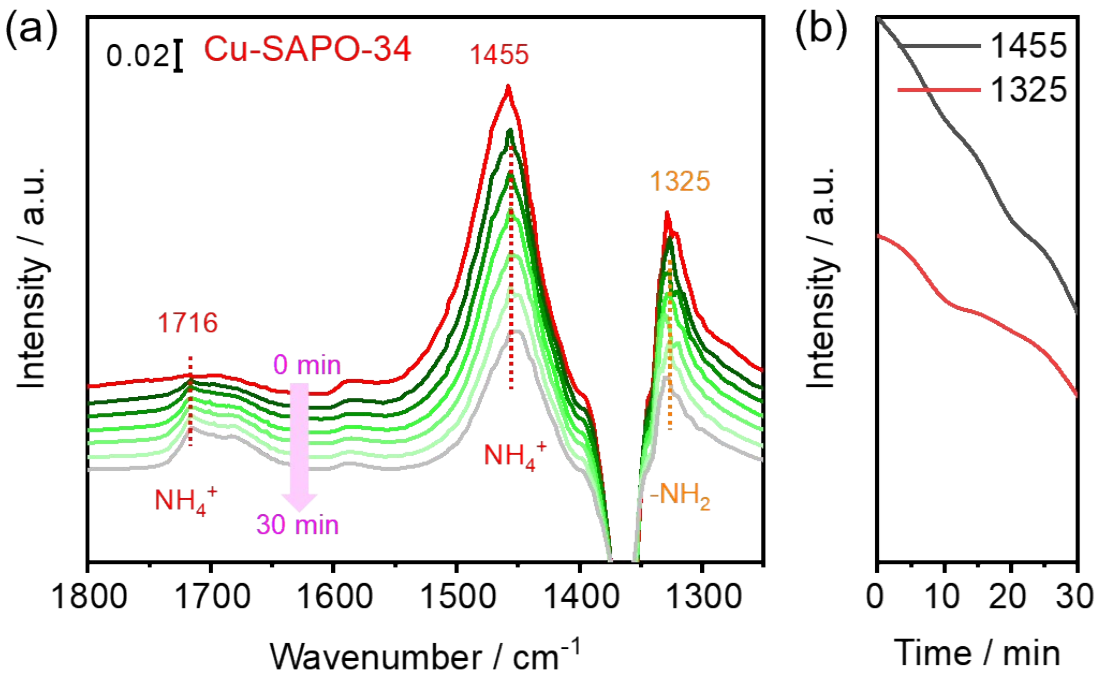

Figure S23. *In situ* DRIFTs of the transient reactions at 250 °C over Cu-SAPO-34 catalyst between $NO+SO_2+O_2$ (a) and preadsorbed NH_3 as a function of time. (b) Consumption of the bands at 1325 cm^{-1} and 1455 cm^{-1} over Cu-SAPO-34 catalyst in Figure (a).

When the reaction of $NO+SO_2+O_2$ is introduced after the adsorption of NH_3, the reactivity of the $-NH_2$ species (1325 cm^{-1}) and the NH_4^+ species (1455 cm^{-1}) is inhibited (Figure S23a, 23b).

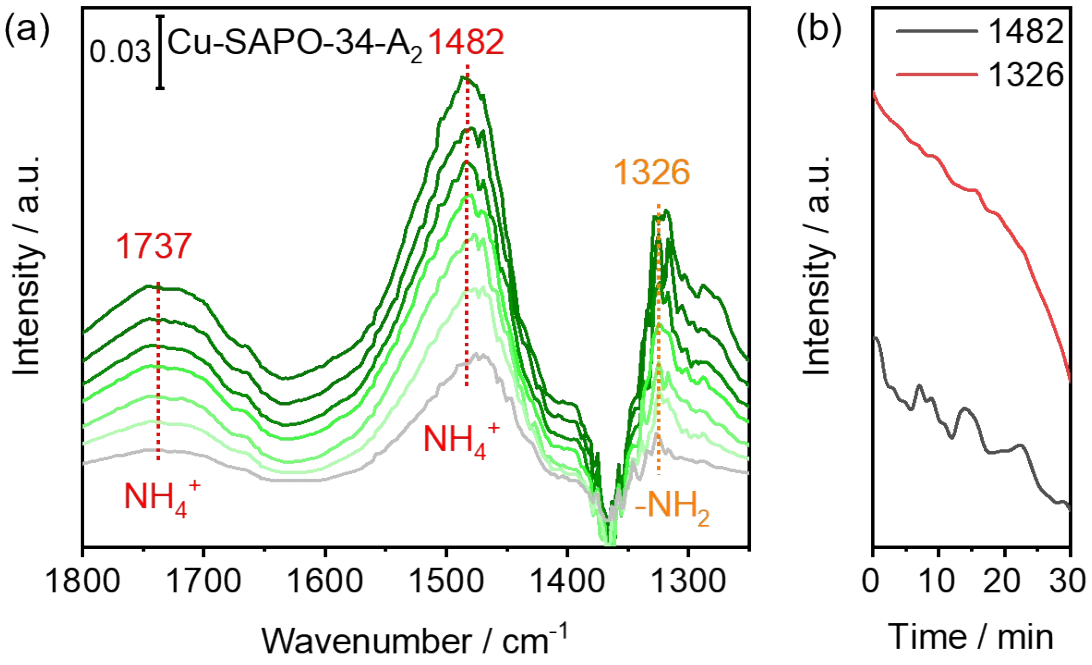

Figure S24. In situ DRIFTs of the transient reactions at 250 °C over Cu-SAPO-34-A_2 catalyst between NO+O_2 (a) and preadsorbed NH_3 as a function of time. (b) Consumption of the bands at 1326 cm^{-1} and 1482 cm^{-1} over Cu-SAPO-34-A_2 catalyst in Figure (a).

Figure S24 shows that the ammonia species on Cu-SAPO-34-A_2 are gradually consumed after the introduction of NO+O_2. After 30 minutes of reaction, the -NH_2 species are basically consumed completely, and the NH_4^+ species consume nearly two thirds.

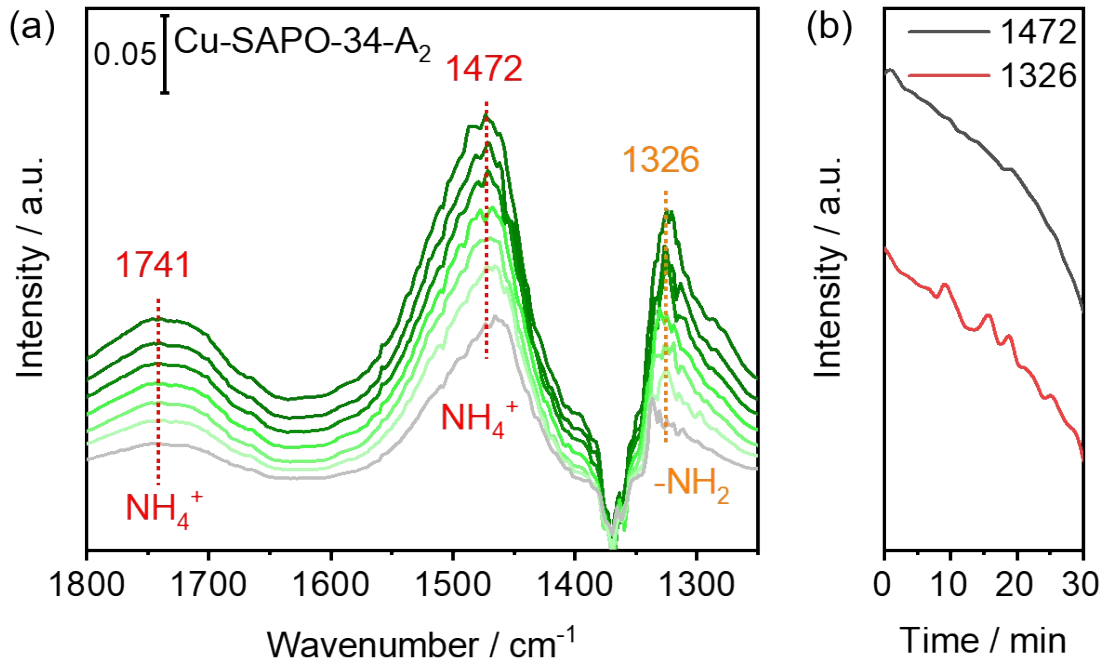

Figure S25. In situ DRIFTs of the transient reactions at 250 °C over Cu-SAPO-34-A_2 catalyst between NO+SO_2+O_2 (a) and preadsorbed NH_3 as a function of time. (b) Consumption of the bands at 1326 cm^{-1} and 1472 cm^{-1} over Cu-SAPO-34-A_2 catalyst in Figure (a).

The reaction activity of -NH_2 and NH_4^+ species was inhibited when NO+SO_2+O_2 was introduced into Cu-SAPO-34-A_2 after absorbing NH_3 (Figure S24). After 30 minutes of reaction, -NH_2 species consumed nearly two-thirds, while NH_4^+ species consumed only half.

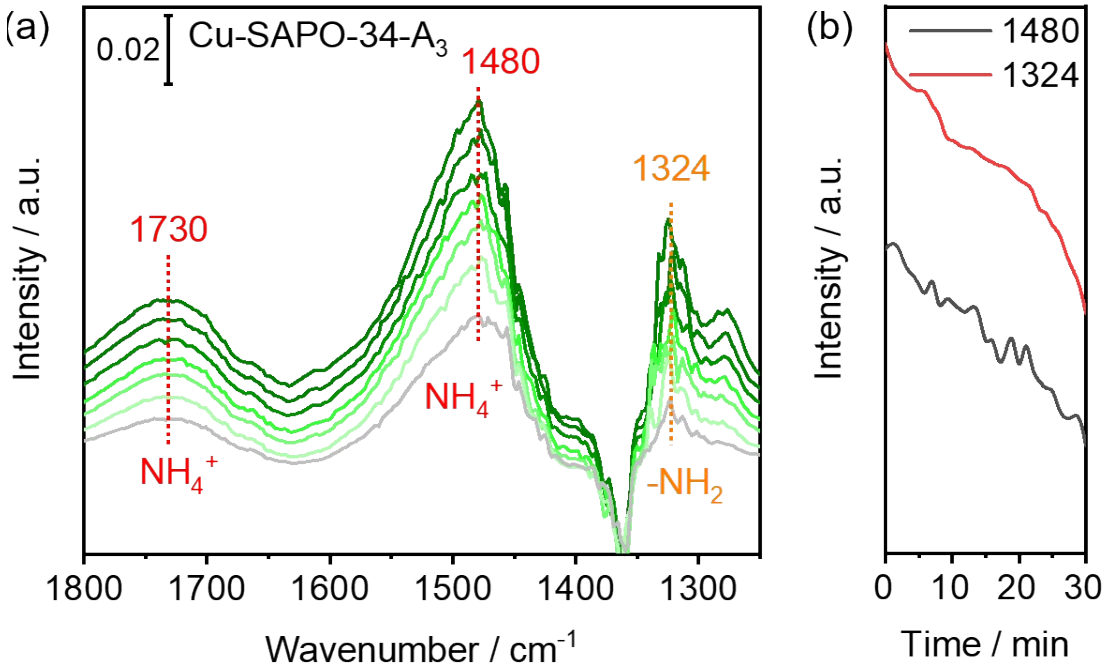

Figure S26. In situ DRIFTs of the transient reactions at 250 °C over Cu-SAPO-34-A_3 catalyst between $NO+O_2$ (a) and preadsorbed NH_3 as a function of time. (b) Consumption of the bands at 1324 cm^{-1} and 1480 cm^{-1} over Cu-SAPO-34-A_3 catalyst in Figure (a).

Figure S26 shows that the ammonia species adsorbed on Cu-SAPO-34-A_3 is slowly consumed after the introduction of $NO+O_2$. After 30 minutes of reaction, the -NH_2 species consume two-thirds and the NH_4^+ species only half.

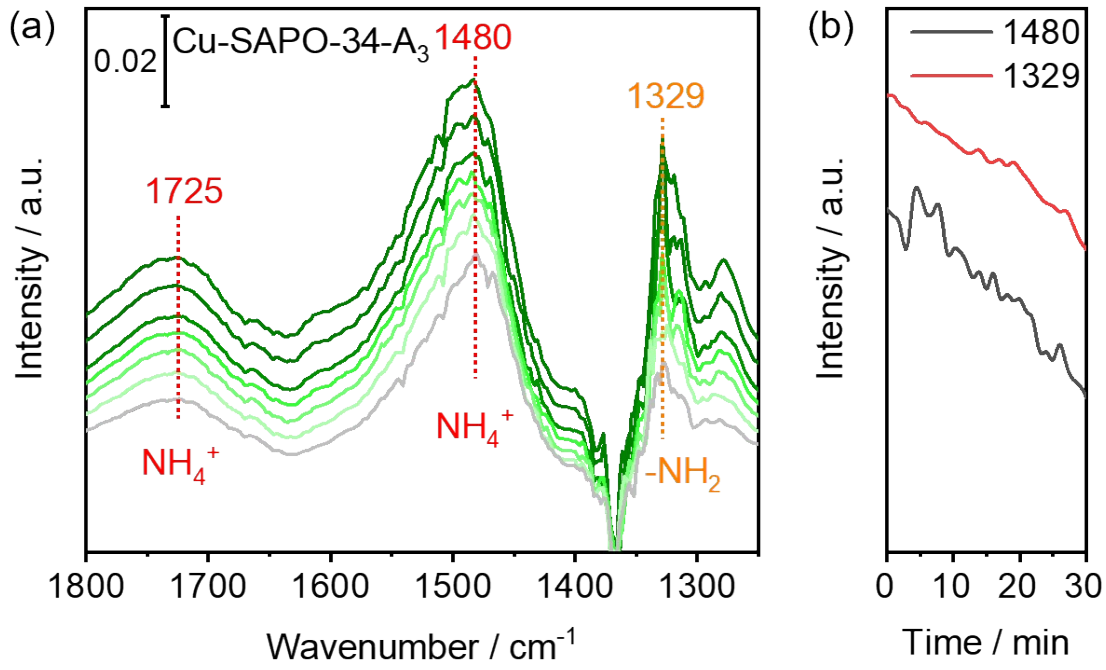

Figure S27. In situ DRIFTs of the transient reactions at 250 °C over Cu-SAPO-34-A_3 catalyst between NO+SO_2+O_2 (a) and preadsorbed NH_3 as a function of time. (b) Consumption of the bands at 1329 cm^{-1} and 1480 cm^{-1} over Cu-SAPO-34-A_3 catalyst in Figure (a).

When the reaction atmosphere is adjusted to NO+SO_2+O_2, the reactivity of -NH_2 and NH_4^+ is further inhibited (Figure S27). After 30 minutes of reaction, the consumption of -NH_2 species is less than two-thirds, and that of NH_4^+ species is only about one-third.

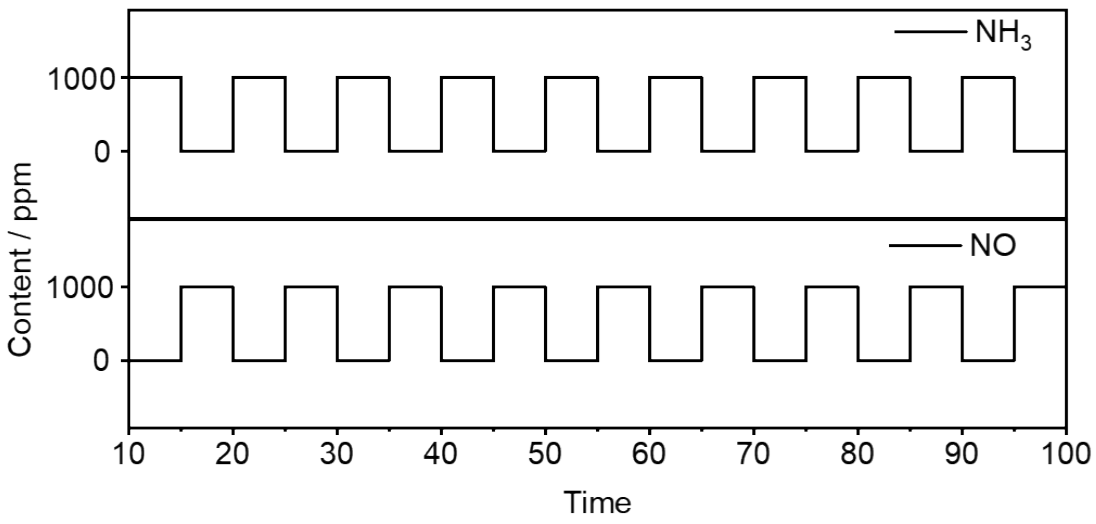

Figure S28. Schematic illustration of gases alternation for NH_3/NO in the pulsed DRIFTs experiments.

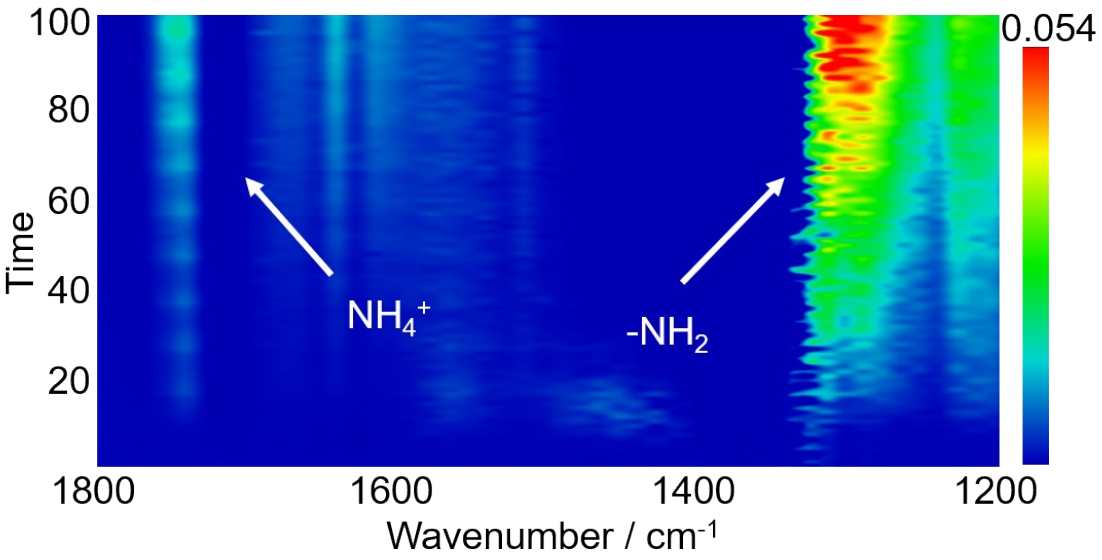

Figure S29. Mapping picture of pulse DRIFTs spectra of SO_2-poisoned Cu-SAPO-34-A-S catalysts obtained at 250 °C before the pretreated at 300 °C.

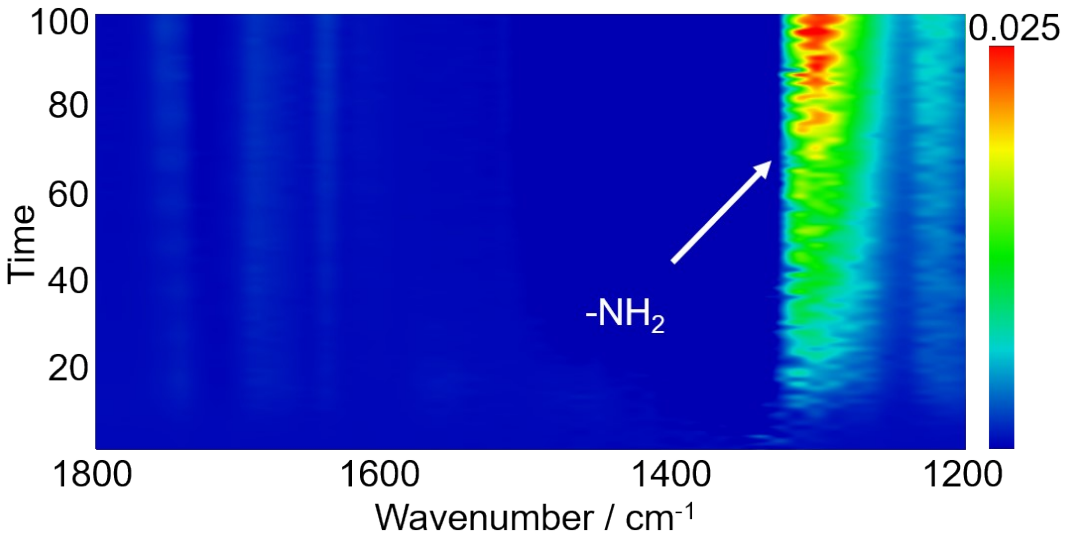

Figure S30. Mapping picture of pulse DRIFTs spectra of SO_2-poisoned Cu-SAPO-34-S catalysts obtained at 250 °C before the pretreated at 300 °C.

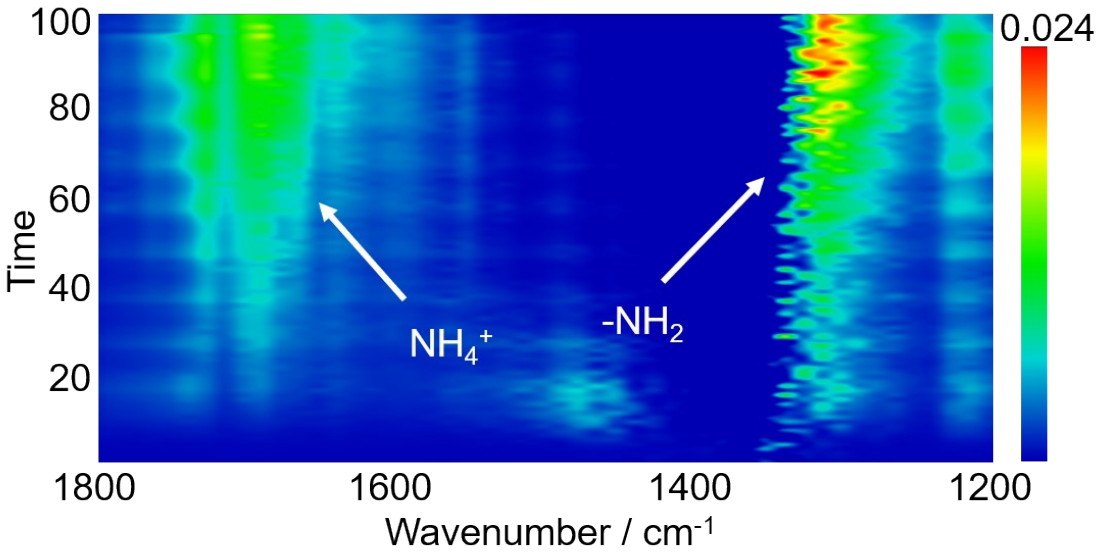

Figure S31. Mapping picture of pulse DRIFTs spectra of SO_2-poisoned Cu-SAPO-34-A-S catalysts obtained at 250 °C before the pretreated at 350 °C.

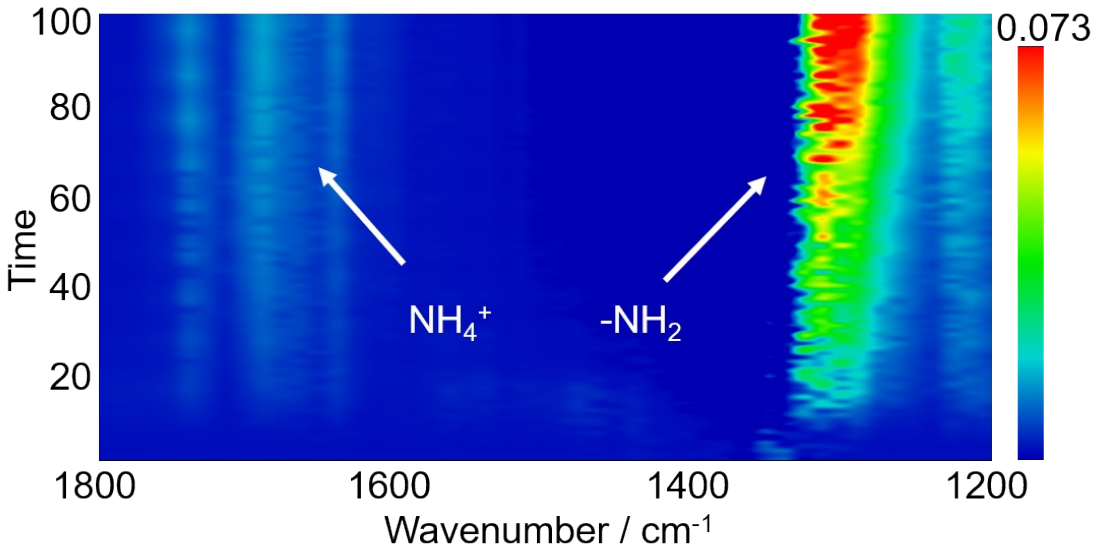

Figure S32. Mapping picture of pulse DRIFTs spectra of SO_2-poisoned Cu-SAPO-34-S catalysts obtained at 250 °C before the pretreated at 350 °C.

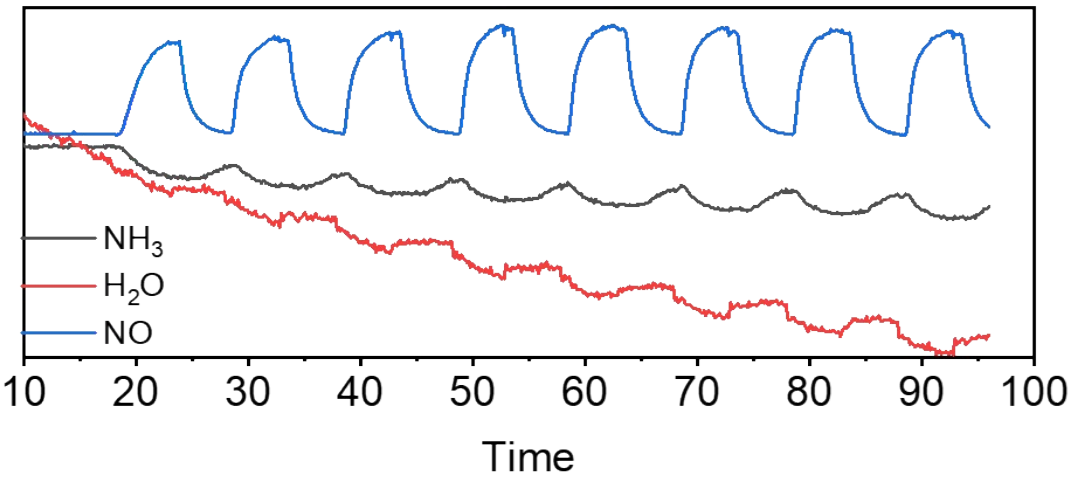

Figure S33. Mass spectrometry plots on NH_3, NO and H_2O versus time in the exhaust gas of pulse DRIFTs spectra of Cu-SAPO-34-A-S catalysts which were obtained at 250 °C before the pretreatment at 300 °C.

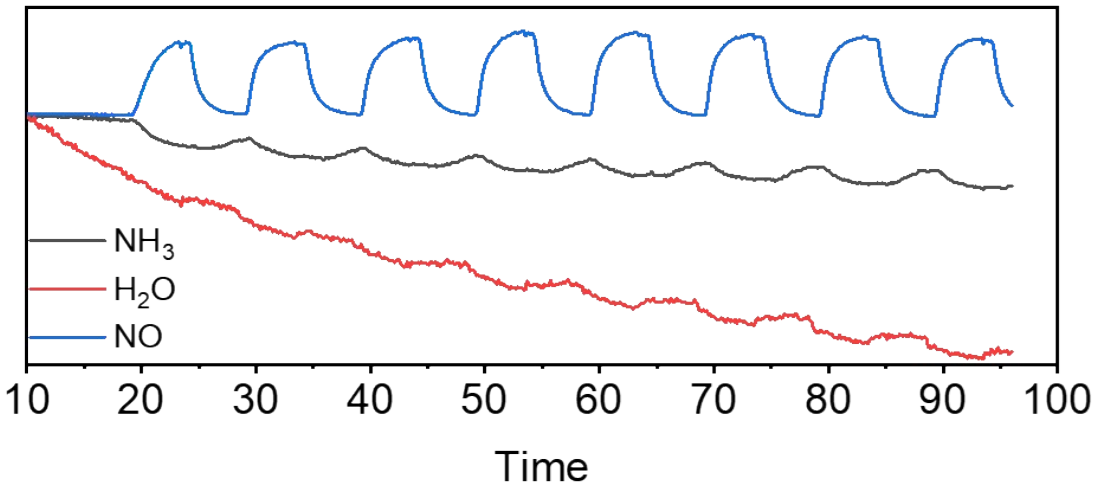

Figure S34. Mass spectrometry plots on NH_3, NO and H_2O versus time in the exhaust gas of pulse DRIFTs spectra of Cu-SAPO-34-S catalysts which were obtained at 250 °C before the pretreatment at 300 °C.

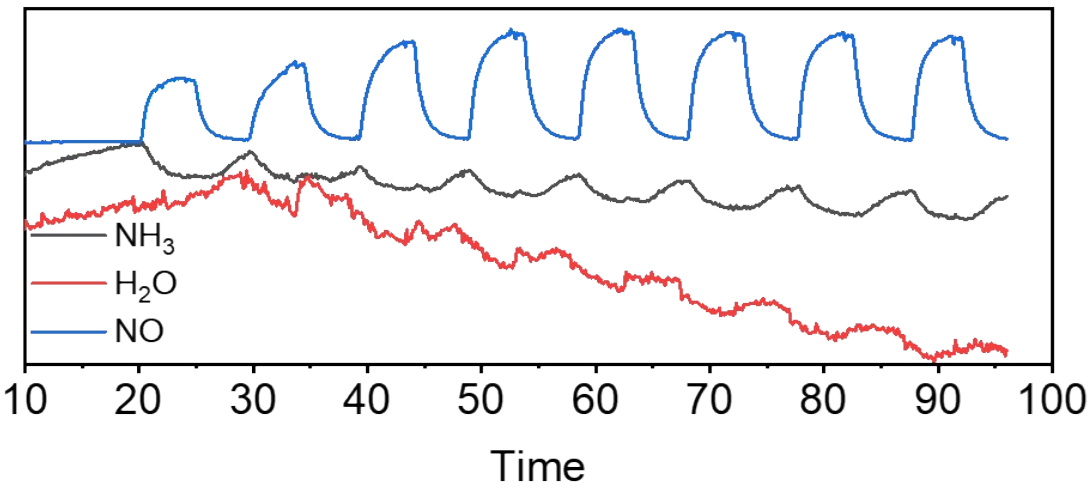

Figure S35. Mass spectrometry plots on NH_3, NO and H_2O versus time in the exhaust gas of pulse DRIFTs spectra of Cu-SAPO-34-A-S catalysts which were obtained at 250 °C before the pretreatment at 350 °C.

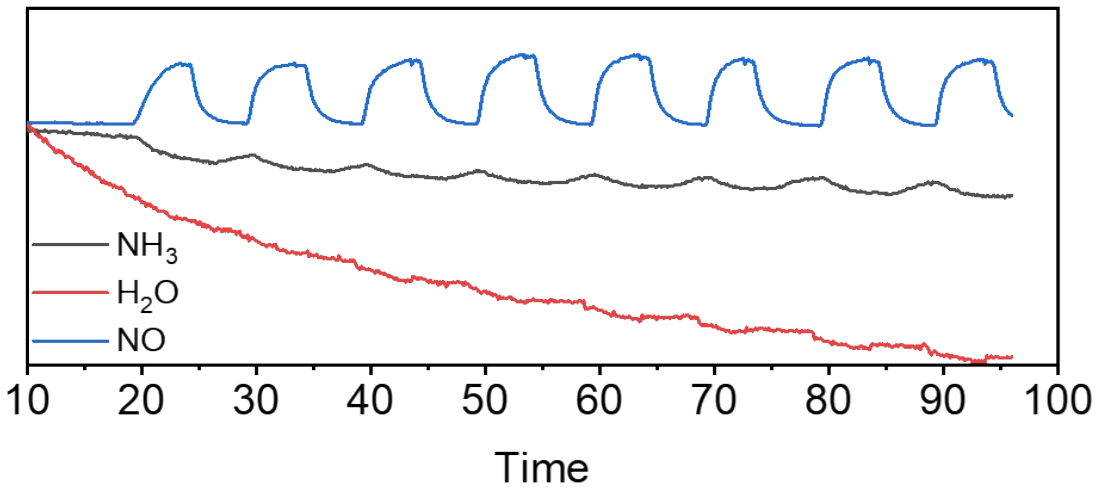

Figure S36. Mass spectrometry plots on NH_3, NO and H_2O versus time in the exhaust gas of pulse DRIFTs spectra of Cu-SAPO-34-S catalysts which were obtained at 250 °C before the pretreatment at 350 °C.

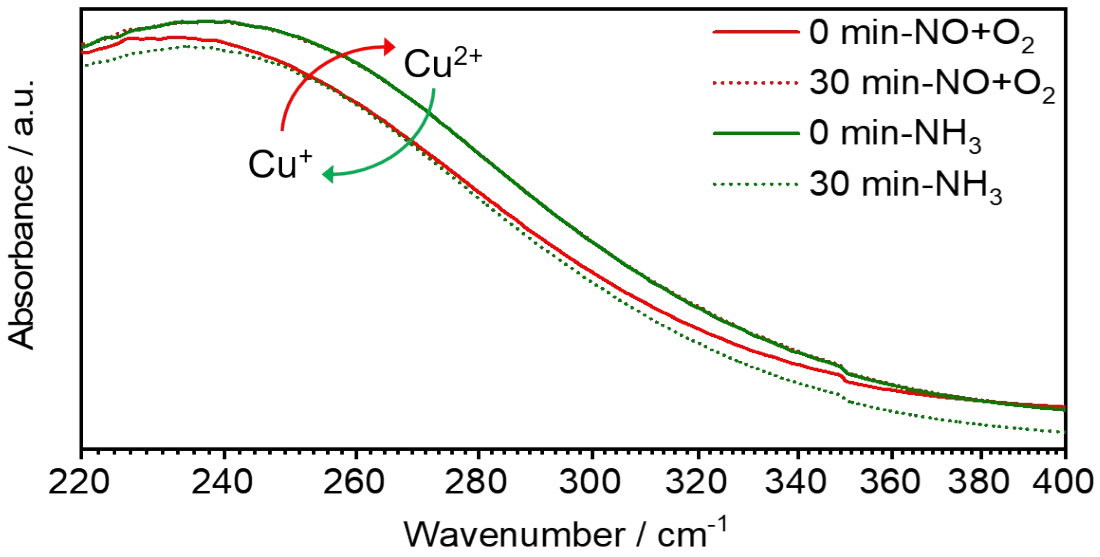

Figure S37. *In situ* UV-vis spectra of oxidation and reduction half-reaction of the Cu-SAPO-34-A catalyst at 250 °C. The oxidizing feed is 1000 ppm $NO+O_2$, the reduction feed is 1000 ppm NH_3.

In Figure S37, the Cu sites in the Cu-SAPO-34-A are oxidized to Cu^{II} in the $NO+O_2$ atmosphere, and the oligonuclear $[Cu\text{-}O\text{-}Cu]_n$ species are more easily formed. After the introduction of NH_3, the Cu^{II} content drops to the initial state, and the oligonuclear $[Cu\text{-}O\text{-}Cu]_n$ species content also drops to the state of 0 min-$NO+O_2$.

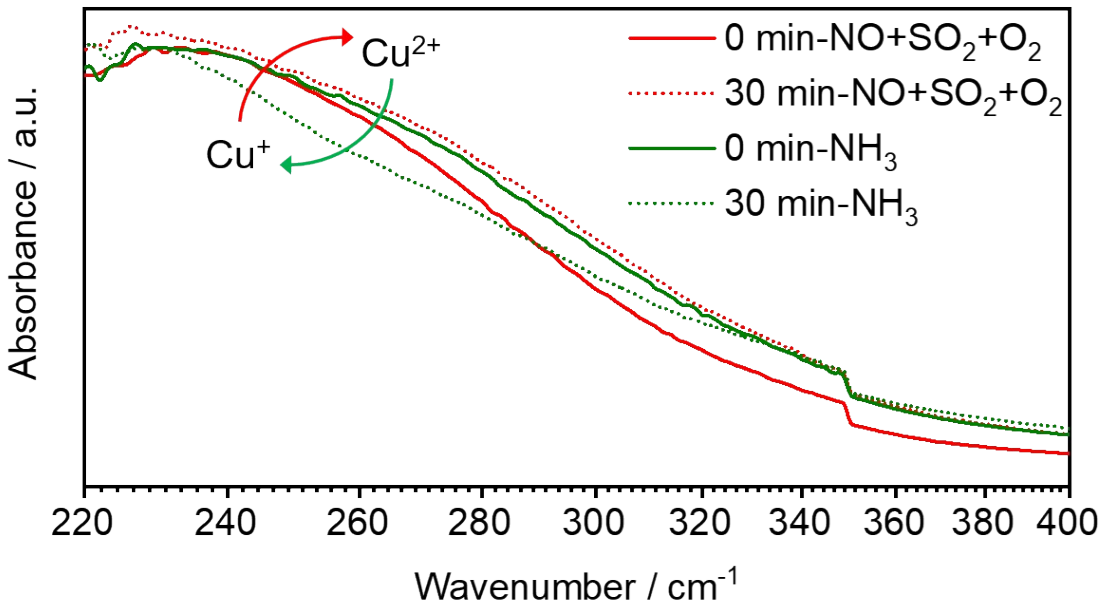

Figure S38. *In situ* UV-vis spectra of oxidation and reduction half-reaction of the Cu-SAPO-34-A catalyst at 250 °C. The oxidizing feed is 1000 ppm NO+1000 ppm SO_2+O_2, and the reduction feed is 1000 ppm NH_3.

However, in Figure S38, the introduction of NO+SO_2+O_2 cause Cu species to be oxidized to Cu^{II}, the content of oligonuclear $[Cu\text{-}O\text{-}Cu]_n$ species increase, and subsequent NH_3 reduction also restore the original state.

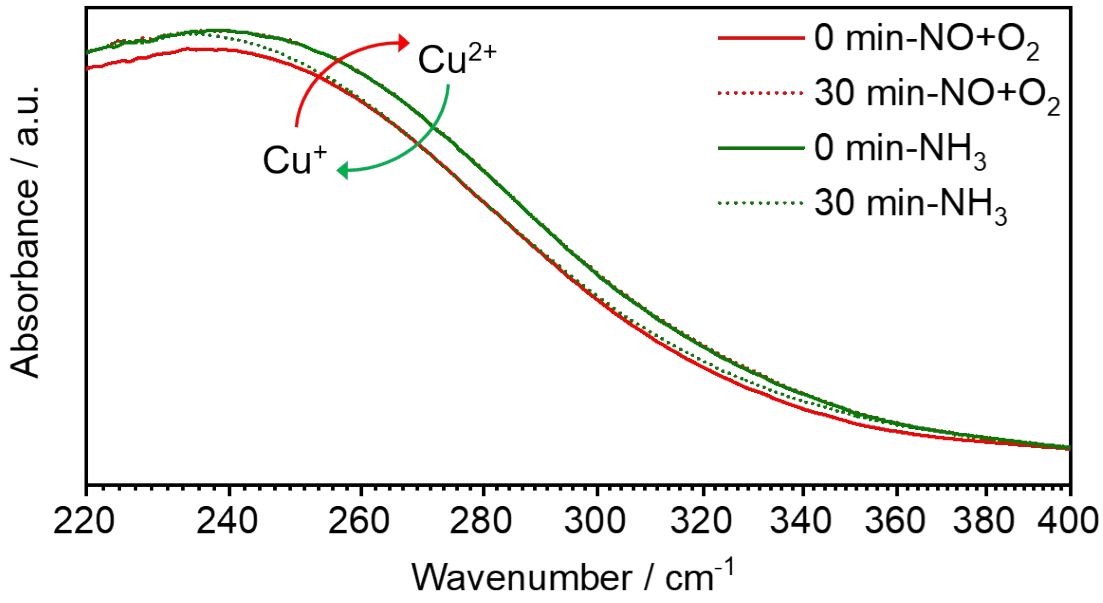

Figure S39. *In situ* UV-vis spectra of oxidation and reduction half-reaction of the Cu-SAPO-34 catalyst at 250 °C. The oxidizing feed is 1000 ppm $NO+O_2$, the reduction feed is 1000 ppm NH_3.

Figure S39 shows that on the Cu-SAPO-34, the Cu species are oxidized and polymerized under the $NO+O_2$ feed, and then reduced to the initial state in the NH_3 atmosphere. The oxidation and reduction reaction maintains a balance, thereby ensuring the efficiency of the SCR reaction.

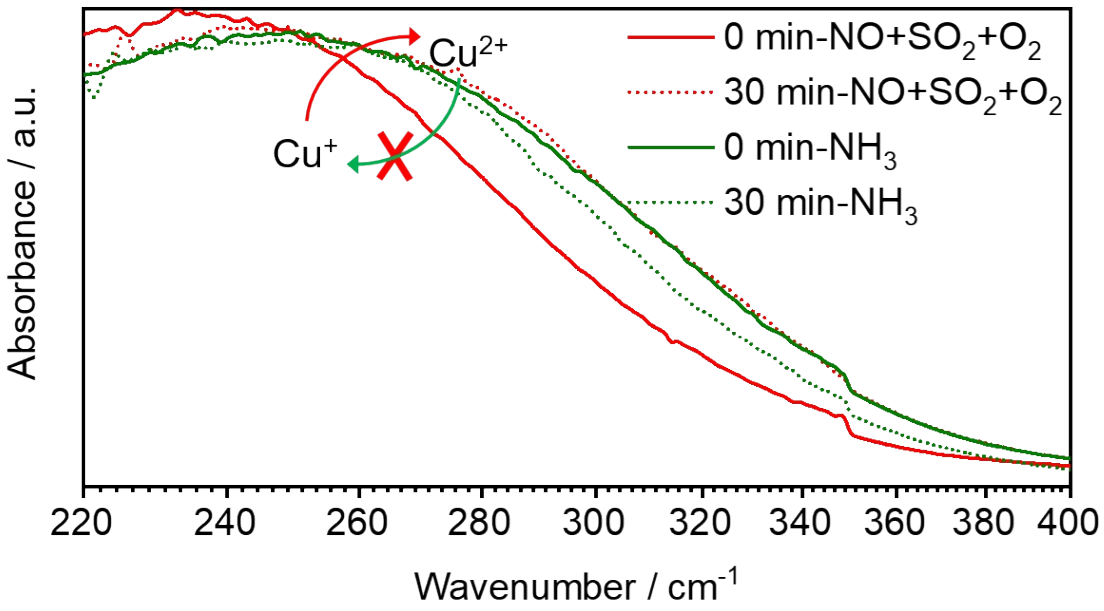

Figure S40. *In situ* UV-vis spectra of oxidation and reduction half-reaction of the Cu-SAPO-34 catalyst at 250 °C. The oxidizing feed is 1000 ppm NO+1000 ppm SO_2+O_2, the reduction feed is 1000 ppm NH_3.

In Figure S40, the Cu sites on the Cu-SAPO-34 are oxidized to Cu^{II} sites in the feed of NO+SO_2+O_2. Compared with Figure S39, it can be observed that the content of Cu^{II} sites is greatly increased, indicating that the introduction of SO_2 has strengthened the oxidation of oxidizing atmosphere (NO+SO_2+O_2). This also makes it difficult to reduce Cu^{II} and oligonuclear $[Cu\text{-}O\text{-}Cu]_n$ species after the subsequent introduction of NH_3.

Table S1. The content of Z_2Cu and ZCuOH sites in Cu-SAPO-34 and Cu-SAPO-34-A catalysts calibrated by H_2-TPR and ammonia titration.

	The content	The content of	The content	The content of

	of Z_2Cu / % [a]	ZCuOH / % [a]	of Z_2Cu / % [b]	ZCuOH / % [b]
Cu-SAPO-34	10.1	89.9	10.0	90.0
Cu-SAPO-34-A	23.4	76.6	23.5	76.5

[a]* represents the data of H_2-TPR, and [b]* represents the data of ammonia titration method.

Table S2. O, Al, Cu and S elements content in Cu-SAPO-34, Cu-SAPO-34-A, Cu-SAPO-34-S and Cu-SAPO-34-A-S catalysts.

	O/%		Al/%		Cu/%		S/%	
	a*	b*	a*	b*	a*	b*	a*	b*
Cu-SAPO-34	60.4	56.1	18	19.0	2.6	1.7	/	/
Cu-SAPO-34-A	59.2	55	18.1	20.4	2.0	1.6	/	/
Cu-SAPO-34-S	60.8	56.8	17.4	19.4	2.1	1.7	0.6	0.5
Cu-SAPO-34-A-S	59.2	57.6	18.1	18.6	1.8	1.8	0	0.3

a* represents the data of flat scanning, and b* represents the data of EDX.

Table S3. The specific breakthrough time and SO_2 adsorption capacity of various catalysts.

	200 °C		300 °C	
	Break through time / s	SO_2 ads- capacity / mmol·g^{-1}	Break through time / s	SO_2 ads- capacity / mmol·g^{-1}
Cu-SAPO-34	83.7	0.050	84.7	0.030
Cu-SAPO-34-A	66.0	0.032	32.0	0.020

Table S4. Adsorption energy and adsorption distance of NH_3, NO, SO_2 and competitive adsorption of NO with SO_2.

	NH_3		NO		SO_2		NO and SO_2	
	α*	β*	α*	β*	α*	β*	β* of NO	β* of SO_2
Z_2Cu	-1.04	2.000	-0.45	1.962	-0.30	2.334	1.961	2.647
ZCuOH	-1.05	2.005	-0.22	3.581	-0.53	1.948[1] 1.919[2]	3.878	1.973[1] 1.830[2]

α* represents the data of Adsorption energy (eV), and β* represents the Adsorption distance (Å); [1] represents the data of the adsorption distance from the O atom of SO_2 to the Cu atom, and [2] represents the the adsorption distance from the S atom of SO_2 to the O atom.

Table S5. The deposition quality of sulfate species on Cu-SAPO-34-A and Cu-SAPO-34 catalysts.

	(The amount of sulfate / mmol/g)[1]		(The amount of sulfate / mmol/g)[2]
	metal sulfate species	ABS	metal sulfate species
Cu-SAPO-34	19.0	19.0	11.9
Cu-SAPO-34-A	17.0	13.4	11.9

[1] represents the sulfation condition of SO_2+O_2, as shown in Figure S11a, S11b;

[2] represents the sulfation condition of SO_2+NH_3+O_2, as shown in Figure S 11c, 11d.

References

1. J. P. Perdew, K. Burke and M. Ernzerhof, Generalized gradient approximation made simple *Phys. Rev. Lett*, 1997, **78**, 1396-1396.
2. G. Kresse and J. Hafner, Ab initio molecular dynamics for liquid metals, *Phys. Rev. B*, 1993, **47**, 558-561.
3. N. Troullier and J. L. Martins, Efficient pseudopotentials for plane-wave calculations, *Phys. Rev. B*, 1991, **43**, 1993-2006.
4. Y. Jangjou, Q. Do, Y. Gu, L.-G. Lim, H. Sun, D. Wang, A. Kumar, J. Li, L. C. Grabow and W. S. Epling, Nature of Cu Active Centers in Cu-SSZ-13 and Their Responses to SO_2 Exposure, *ACS Catalysis*, 2018, **8**, 1325-1337.
5. W. Su, Z. Li, Y. Peng and J. Li, Correlation of the changes in the framework and active Cu sites for typical Cu/CHA zeolites (SSZ-13 and SAPO-34) during hydrothermal aging, *Phys Chem Chem Phys*, 2015, **17**, 29142-29149.
6. Y. Wan, G. Yang, J. Xiang, X. Shen, D. Yang, Y. Chen, V. Rac, V. Rakic and X. Du, Promoting effects of water on the NH_3-SCR reaction over Cu-SAPO-34 catalysts: transient and permanent influences on Cu species, *Dalton Trans*, 2020, **49**, 764-773.
7. S. Zhou, F. Tang, H. Wang, S. Wang and L. Liu, Effect of Cu Concentration on the Selective Catalytic Reduction of NO with Ammonia for Aluminosilicate Zeolite SSZ-13 Catalysts, *The Journal of Physical Chemistry C*, 2021, **125**, 14675-14680.
8. B. Chen, R. Xu, R. Zhang and N. Liu, Economical way to synthesize SSZ-13 with abundant ion-exchanged Cu^+ for an extraordinary performance in selective catalytic reduction (SCR) of NOx by ammonia, *Environ Sci Technol*, 2014, **48**, 13909-13916.
9. X. Liu, X. Wu, D. Weng, Z. Si and R. Ran, Evolution of copper species on Cu/SAPO-34 SCR catalysts upon hydrothermal aging, *Catalysis Today*, 2017, **281**, 596-604.
10. N. Zhu, Z. Lian, Y. Zhang, W. Shan and H. He, The promotional effect of H_2 reduction treatment on the low-temperature NH_3-SCR activity of Cu/SAPO-18, *Applied Surface Science*, 2019, **483**, 536-544.

11. H. Wang, X. Xu, J. Hao, P. Ning and Q. Zhang, Unravelling the phosphorus-induced effect on NH_3-SCR catalytic performance, hydrothermal stability and SO_2 resistance of Cu/SAPO-34, *Applied Catalysis A: General*, 2022, **646**.

12. Y. Ma, S. Cheng, X. Wu, T. Ma, L. Liu, B. Jin, M. Liu, J. Liu, R. Ran, Z. Si and D. Weng, Improved hydrothermal durability of Cu-SSZ-13 NH_3-SCR catalyst by surface Al modification: Affinity and passivation, *Journal of Catalysis*, 2022, **405**, 199-211.

13. A. G. Greenaway, A. Marberger, A. Thetford, I. Lezcano-Gonzalez, M. Agote-Aran, M. Nachtegaal, D. Ferri, O. Krocher, C. R. A. Catlow and A. M. Beale, Detection of key transient Cu intermediates in SSZ-13 during NH_3-SCR deNO_x by modulation excitation IR spectroscopy, *Chem Sci*, 2020, **11**, 447-455.

14. S. Zhang, J. Chen, Y. Meng, L. Pang, Y. Guo, Z. Luo, Y. Fang, Y. Dong, W. Cai and T. Li, Insight into solid-state ion-exchanged Cu-based zeolite (SSZ-13, SAPO-18, and SAPO-34) catalysts for the NH_3-SCR reaction: The promoting role of NH_4-form zeolite substrates, *Applied Surface Science*, 2022, **571**.

15. H. Zhu, J. H. Kwak, C. H. F. Peden and J. Szanyi, In situ DRIFTS-MS studies on the oxidation of adsorbed NH_3 by NO_x over a Cu-SSZ-13 zeolite, *Catalysis Today*, 2013, **205**, 16-23.

16. Y. Li, J. Deng, W. Song, J. Liu, Z. Zhao, M. Gao, Y. Wei and L. Zhao, Nature of Cu Species in Cu–SAPO-18 Catalyst for NH_3–SCR: Combination of Experiments and DFT Calculations, *The Journal of Physical Chemistry C*, 2016, **120**, 14669-14680.

17. L. Ma, Y. Cheng, G. Cavataio, R. W. McCabe, L. Fu and J. Li, In situ DRIFTS and temperature-programmed technology study on NH_3-SCR of NO over Cu-SSZ-13 and Cu-SAPO-34 catalysts, *Applied Catalysis B: Environmental*, 2014, **156-157**, 428-437.